SEDIMENT TRANSPORT ON TRANSVERSELY SLOPING BEDS IN A CAROUSEL

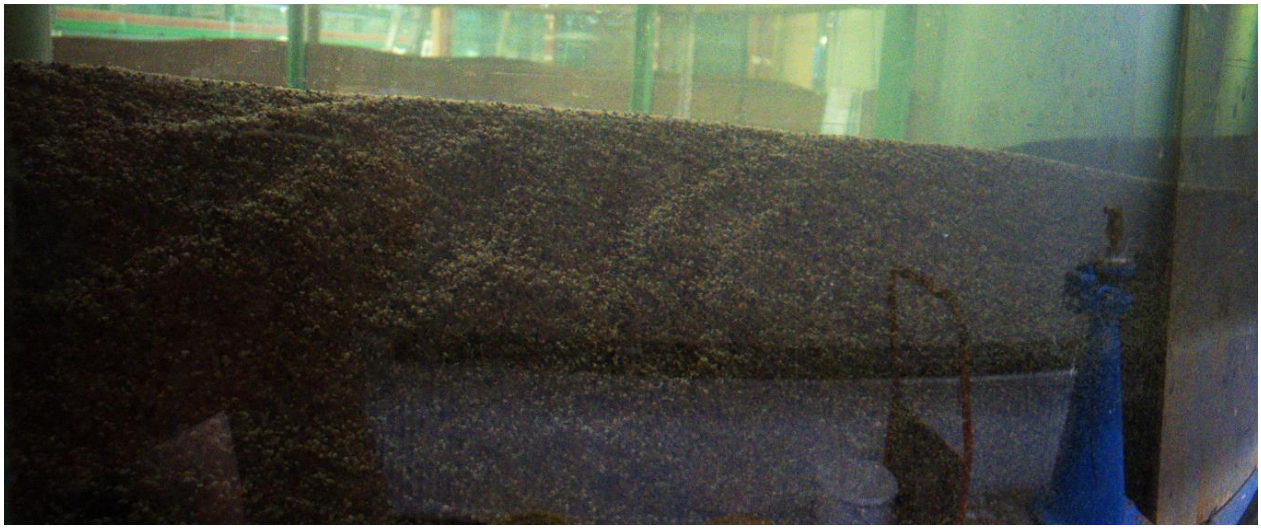

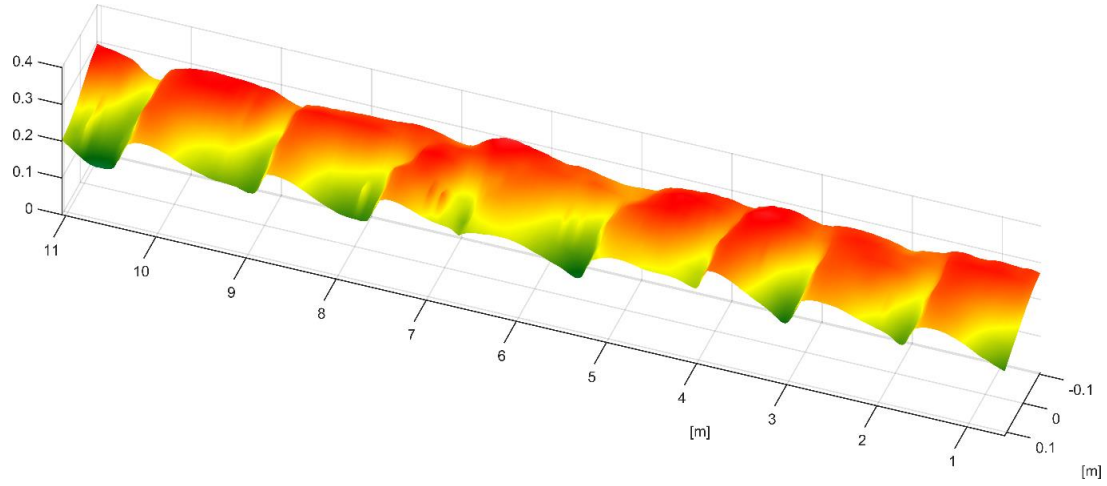

MSc. Thesis Earth Sciences
J.C. de Smit
Utrecht University, Department of Physcial Geography
Student number: 3849538
Supervisors: Prof. Dr. M.G. Kleinhans
A.W. Baar, Msc.
In cooperation with Prof. W. Uijttewaal (TU Delft)
2016-02-07

ABSTRACT

The transverse slope effect is one of the most important parameters in the modelling of fluvial morphology. It determines to a large extent the properties and patterns of channels and bars, bifurcation stability, and grain sorting. Quantification of the transverse slope effect has been realized by mathematical modelling in combination with bed levelling experiments in straight and curved flumes. Though an inverse dependence on the square root of Shields' number is generally accepted, current transverse slope predictors contain multiple calibration factors due to a lack of experimental data and limitations in chosen transport conditions. In this thesis experiments are conducted in a carousel with of which the lid and floor can be rotated independently, which allows the generation of a wide range of secondary flow intensities. This ability leads to the possibility of conducting experiments under a much wider range of morphological conditions compared to regular flumes, as different bend radii and straight channels can be simulated. The presence of helical flow allows the self-formation of a transverse slope. Over 100 experiments were conducted using 1mm or 4mm grains. The resulting bed slope effect was derived from bed elevation measurements in combination with 1D calculation of helical flow. The results show a large dependence of the transverse slope effect on sediment transport mode. Transition from rolling sediment to saltation led to an increase in magnitude and a lower sensitivity to Shields' number. Similarity of the transverse slope effect between grain sizes was found by relating the slope effect to the ratio between Shields' number and the critical Shields number of sediment transport initiation. Because of the effect of bed forms on local helical flow intensity, and the resulting nonlinear effects on cross channel sediment transport and local transverse slope steepness, a 3D flow model should be used in further research on the bed slope effect in carousels.

TABLE OF CONTENTS AND LIST OF FIGURES

1 INTRODUCTION AND REVIEW

1.1 INTRODUCTION

Fluvial morphology is the result of the continuous interaction between flow and morphology. The nonlinear relation between flow and sediment transport leads to the formation of channels and bars, which in turn change flow and subsequently influence sediment transport and bed topography. This morphodynamic feedback loop (Figure 1) is the basis of the modelling of fluvial systems. The focus of this research is on the transverse slope effect which can be classified in the sediment transport process. This strongly influences bed topography (Schuurman et al., 2013). A tendency currently exists in morphological modelling to use the transverse slope effect as a tuning parameter in the calibration of model results to existing morphology. This is caused by the presence of at least two empirical factors in transverse slope models. Moreover, the influence of bed forms and different sediment transport modes is currently not accounted for. The aim of this study is to derive a new transverse slope predictor on the basis of a large dataset from experiments in a carousel. The wide range of chosen flow conditions provides data on multiple sediment transport modes and a wide range of morphological conditions.

In the next chapter a literature review is given where processes on transverse slopes are described, well known transverse slope predictors are collected, and knowledge gaps and uncertainties are identified. On the basis of these research questions and hypotheses are given. Next the experimental setup and data analysis are described, followed by the results, discussion, conclusions, and recommendations.

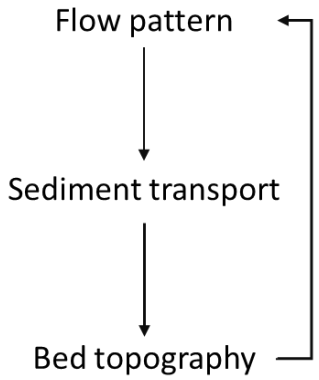

Figure 1, the morphodynamic feedback loop.

1.2 LITERATURE REVIEW

1.2.1 Transverse slope effect

On a sloping bed, the force balance on a grain has a gravity component which is directed parallel to the slope direction. When the slope is parallel to the flow direction, total sediment transport is increased, but it remains to have the same direction as shear stress exerted by flowing water. Except for very steep slopes gravity transport is very small compared to sediment transport by water. Therefore the slope hardly changes the amount of particle motion (Sekine & Parker, 1992). However, bars, banks and bed forms have a transverse slope which causes the sediment transport vector to deflect downslope from the direction of fluid shear stress. The direction of bed load transport over these slopes then consists of a shear stress parallel to the flow, and a perpendicular gravity component. Even when the transverse component is small compared to the shear stress, a perpendicular component will change the net transport direction. This deflection of net sediment transport in the downslope direction plays an important role in river morphology (Struiksma et al., 1985), and is related to many phenomena which are observed in fluvial systems (section 1.2.4).

1.2.2 Processes on transverse slopes, straight channels

Figure 2 shows the force balance of a grain on a transversely sloping bed. The main flow is parallel to the channel, so that the shear stress has no up or downslope component. As the bed is inclined at an angle, the gravitational force F_g has a downslope component acting on the grains. The gravitational pull is perpendicular to the main flow direction and shear stress. Therefore the total transport vector has a downslope angle α in respect to the horizontal. This angle depends on the angle of the bed, which determines $F_{g,downslope}$, and the fluid drag force determined by the flow velocity. Total sediment transport is the sum of these two vectors.

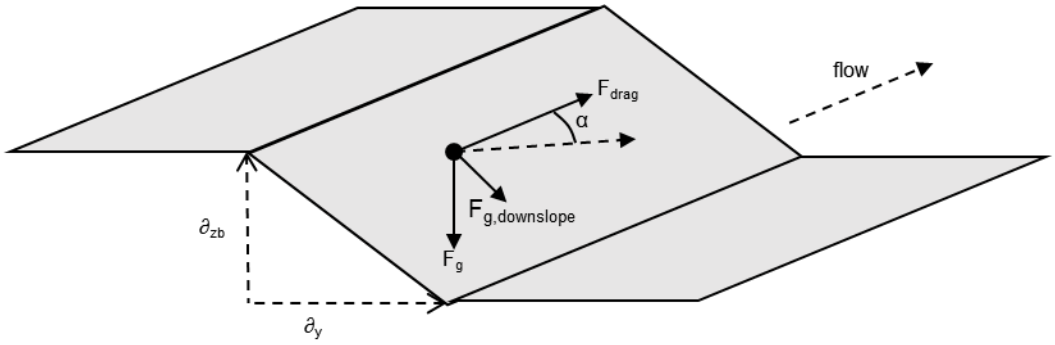

Figure 2, Force balance for a grain on a transversely sloping bed.

The magnitude of the transverse slope effect, so the value of α in Figure 2, is assumed to depend on the transverse bed angle and a function of Shields' number (e.g. Struiksma et al., 1985; Talmon et al., 1995; Talmon and Wiesemann, 2006) as these determine the values of F_g and F_{drag} in the above force balance The general equation for the direction of movement of grains on a sloping bed (Struiksma, 1985) is:

$$\tan(\alpha) = \frac{\sin(\delta) - \frac{1}{f(\theta)}\frac{\partial z_b}{\partial y}}{\cos(\delta) - \frac{1}{f(\theta)}\frac{\partial z_b}{\partial x}} \quad (1)$$

in which α is the direction of sediment transport, δ is the angle of the flow near the bed with x, *x* and *y* are the longitudinal and transverse coordinates respectively, z_b is the bed elevation, and *f*(θ) is a function of Shields' number. For bed load transport, Shields' number is calculated as:

$$\theta = \frac{\tau}{(\rho_s - \rho_w) g D_{50}} \quad (2)$$

where τ is shear stress (N/m^2), ρ_w is the density of water (1000kg/m^3), ρ_s is the sediment density (~2600kg/m^3 for quartz), g is gravitational acceleration (m/s^2), and C is the Chézy coefficient. Shear stress is calculated as:

$$\tau = \rho_w g \left(\frac{u}{C}\right)^2 \quad (3)$$

where u is flow velocity (m/s) and C is the Chézy roughness coefficient.

In the case of a straight channel the water motion is assumed to have no transverse component, so δ is 0. If only the effect on the direction of sediment transport of the slope in the transverse direction is considered, equation (1) is reduced to the following form:

$$\tan(\alpha) = -\frac{1}{f(\theta)}\frac{\partial z_b}{\partial y} \quad (4)$$

From data derived from mathematically from the aforementioned assumptions (e.g. Struiksma, 1985; Struiksma, 1988 in Talmon and De Graaff, 1991), and bed levelling experiments in straight flumes (e.g. Talmon et al., 1995; Wiesemann et al., 2006) where the rate at which a tilted bed relaxes to a horizontal state is measured. f(θ) is determined to be proportional to the square root of Shields' number:

$$f(\theta) = A\sqrt{\theta} \quad (5)$$

where A is an empirical factor (Order 0.5-3). Currently this is the generally accepted form of the transverse bed slope effect which is used in morphological modelling, whereby A is used for calibration.

1.2.3 Processes on transverse slopes, curved channels

The self-formed transverse slope in a curved channel is the result of the balance between the upslope sediment transport by secondary or helical flow, and the transverse slope effect transporting sediment downslope (Odgaard, 1988). Secondary flow is caused by the vertical variation of outward centrifugal forces on the water flowing into a bend (Engelund, 1974). The centrifugal force at the bed is smaller than the

centrifugal force near the water table due to the vertical variation in flow velocity. Since the inwards directed pressure is equal along the vertical, water will flow towards the outer bank near the water table and towards the inner bank near the bed. This results in the formation of a secondary circulation cell (Figure 3).

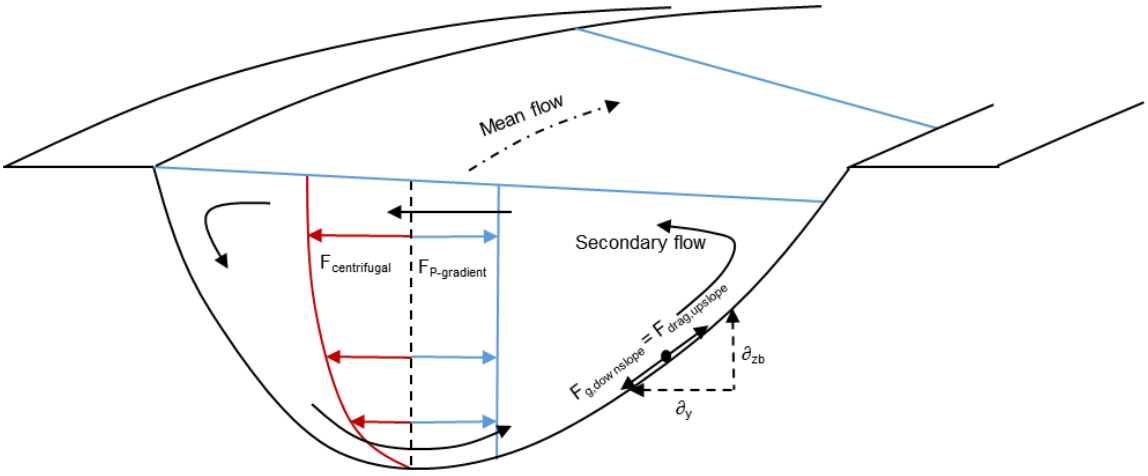

Figure 3, the formation of a secondary circulation cell and self-formed transverse slope in a river bend.

In situations which are in morphological balance, the downslope angle between net sediment transport and mean flow α caused by the transverse slope effect equals the upslope angle δ caused by secondary flow. Thus to obtain the magnitude of the bed slope effect, the upslope transport by secondary flow has to be known. Several predictors for the ratio between helical flow and tangential flow exist (e.g. Engelund, 1974; Ikeda and Nishimura, 1986; Olesen, 1987). This angle does not vary for different mean flow velocities, $u_{secondary}$ scales linearly with u_{mean}, and is assumed to vary little with bed roughness and grain size (Engelund, 1974). It mostly depends on local water depth, bend radius, and the ratio between flow velocity and shear velocity (so the shape of the logarithmic flow profile) in the considered channel. In its most simple form, the angle of helical flow can be calculated as (Engelund, 1974):

$$\tan(\delta) = \beta \frac{h}{r} \qquad (6)$$

where h is local water depth, r the radius of the bend, and β a factor which depends on the local water depth, the relative vertical location respective to the water depth, the shape of the flow velocity profile along the vertical, and bed roughness.

The theory of Engelund is derived from mathematical analysis of fully developed flow in a long, circular, gentle bend. The relations of Ikeda and Nishimura (1986), and Olesen (1987) are derived from mathematical analysis of fully developed flow in gently curved sinuous channels and comparison with experimental data. All predictors further assume two boundary conditions: The shear stress must vanish at the water surface, and the net flow through the vertical must be zero.

1.2.4 Effects of bed slope transport on morphological processes

Downslope transport on a transversely sloped bed is directly linked to bank erosion in straight, self-formed river channels. In a perfectly straight channel, the shear stress vector is directed downstream. Bed load particles on transversely sloping banks will move downslope due to gravity, which leads to bank erosion (Sekine & Parker, 1992). Bed topography in meander bends is also largely influenced by the transverse slope effect (Engelund 1974; Sekine & Parker, 1992). Meander bends are generally characterized by a steep outer bank, a deep outer bend, and a shallower inner bend with a much gentler slope ending in a point bar. The equilibrium bed profile of a meander bend is the result of the balance between upslope sediment transport by secondary flow, and downslope sediment transport by gravity. A stronger transverse slope effect will lead to smoother bar and bank slopes, as more sediment is transported from the bars and banks into the deeper parts of the channel.

When a channel enters a bend, a point bar will form at the inner bend as secondary flow transport sediment inwards. Downstream of the bend, the bed does not adapt immediately to the new morphodynamic equilibrium, it adapts asymptotically. This is characterized by the adaptation length of a bed disturbance (Kleinhans and van den Berg, 2011). In models the adaptation length of a bed disturbance, which greatly influences channel and bar patterns, depends linearly on the magnitude of the transverse slope effect (Struiksma et al., 1985):

$$\lambda_s = \frac{h}{\pi^2}\left(\frac{W}{h}\right)^2 f(\theta) \tag{7}$$

where λ_s is the adaptation length of a bed disturbance (m), and W and h are the channel width and depth (m). A stronger transverse slope effect increases the calculated adaptation length, so that the disturbance of the bed due to a perturbation is damped out more quickly. This means that with a stronger transverse slope effect, a channel is less likely to form alternate bars or start braiding. An overdamped or underdamped state is more likely to occur. A sensitivity analysis by Schuurman et al., 2013 illustrates the effect of the bed slope effect on morphological dynamicity, braiding intensity, and transverse slope steepness on bars and banks (Figure 4). It was found that the bed slope effect had the largest influence on the channel morphology of the tested parameters. A large bed slope effect leads to wider and shallower channels and bigger, smoother bars. The braiding intensity is lower for a stronger bed slope effect due to the wider channels and bars.

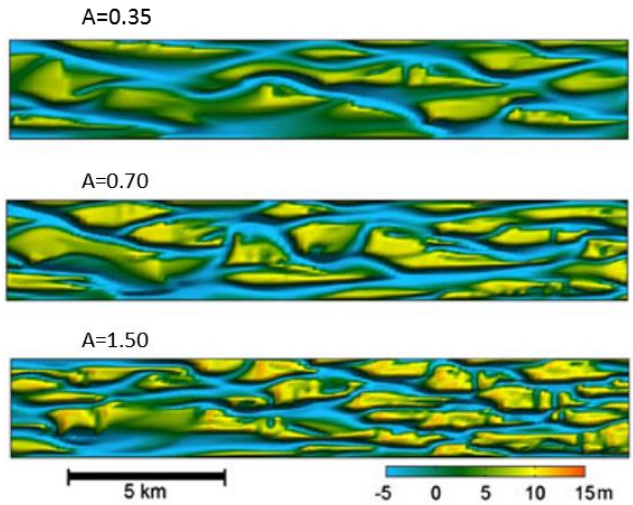

Figure 4, sensitivity analysis for different bed slope effect strengths (A in equation (5), lower A = stronger bed slope effect)) (Schuurman et al., 2013).

The transverse slope effect is known to affect stability of bifurcations (Bolla Pittagula et al., 2003; Miori et al., 2006; Edmonds and Slingerland, 2008; Kleinhans et al., 2008; Kleinhans et al., 2013). Due to the nonlinearity of sediment transport, a bifurcation tends to close off one branch. Water and sediment are distributed proportionally to the widths of the bifurcates (Wang et al., 1995), so at least one channel will always end up receiving more sediment than its transport capacity. As a result one bifurcate will silt up whereas the other deepens, creating a transverse slope just upstream of the bifurcation (Kleinhans et al., 2008). The deflection of sediment transport on that slope will lead to a decrease of sediment feeding into the closing branch and increase sedimentation in the deepening branch. In models, stable bifurcation occurs when sediment transport by gravity along the transverse slope exceeds the excess sediment feed into the closing branch (Bolla Pittagula et al., 2015). This situation can occur for sand bed rivers with symmetrical bifurcations under very high Shields numbers and in asymmetrical bifurcations under moderate Shields numbers (Bolla Pittagula et al., 2015). In models, a different factor A will change the stable state of a bifurcation.

1.2.5 Saltation and suspended sediment

In the transverse slope predictors introduced above it is assumed that only bed load sediment transport is affected by the transverse slope effect. Only particles located on the bed will experience the downslope gravity component as depicted in Figure 2. On the basis of this mechanism it has been argued that transverse slope predictors can only be used for the case of rolling or sliding particles, and are therefore not applicable to saltation (Dietrich and Smith, 1984). But saltating particles are in frequent contact with the bed, and therefore they are regularly subjected to a downslope gravitational force, and thus the transport direction must be deflected. The movement of sediment particles bouncing up and down from a transversely sloping bed has been described and calculated by Sekine and Parker, 1992. An average particle bounce on a flat bed is considered, with each bounce a transverse component is added to its velocity. Subsequent

bounces add more transverse momentum to the particle making each bounce longer and directed more in the transverse direction. In the real world there are some limits to this situation. In flowing water, a particle will always have a longitudinal component giving it momentum. Therefore there will be a limit on the angle of deflection in the transverse direction. Secondly, collisions with the bed are inelastic, and the bed is rough. Therefore the bed is less efficient in generating a downslope component to the trajectory of the particle compared to a smooth bed, and there is a net loss of momentum for each bounce due to inelasticity. On the basis of these assumptions and observations a transverse slope transport relation was developed on the basis of a saltation model (Sekine and Parker, 1992; Sekine and Kikkawa, 1992). The transverse slope effect on saltating particles can be calculated by (Sekine and Parker, 1992):

$$\tan(\alpha) = -0.75\left(\frac{\theta_{cr}}{\theta}\right)^{\frac{1}{4}}\frac{\partial z_b}{\partial y} \qquad (8)$$

where θ_{cr} is the critical Shields number for the initiation of sediment motion. Though this relation was found to predict transverse slope transport accurately through comparison with experimental data of transport by air (Yamasaka et al., 1984) and water (Ikeda, 1982; Hasegawa, 1981; Hirano, 1973), there are some limitations. One of the assumptions in this predictor is that the concentration of saltating grains is low, and therefore it is assumed that grains do not collide. Therefore this predictor cannot be applied for high Shields numbers, as the number of grain collisions would be too high to ignore its effect on sediment transport.

When sediment is in suspension, only the local flow conditions make up the force balance acting on the grains. As the downslope gravitational force component vanishes when contact with the bed is lost. But from experimental data under conditions where suspension occurs has to be concluded that the transverse slope effect and suspended sediment do influence each other somehow, as the introduction of suspended load led to a large scatter (Figure 5; Talmon et al., 1995). This raises the question whether the transverse slope effect is simply larger for situations with a large suspended sediment fraction, or that the transverse slope effect also works on suspended sediment (Talmon and De Graaff, 1991; Talmon et al., 1995). There is no transverse component due to the bed slope on the force balance of the suspended particles. Therefore the transverse slope effect can only work on suspended sediment if the particles are regularly in contact with the bed (Talmon, 1992). This shows similarity to the considerations of Sekine and Parker (1992). A correlation between grain size and transverse bed slope effect for situation with a large suspended fraction is visible in Figure 5, so the particle diameter must be of importance. A dependence to the terminal fall velocity of the particles is expected. Terminal fall velocity is proportional to grain size, larger grains have a higher fall velocity. Taking in account the concepts introduced in Sekine and Parker, 1992, the downslope migration velocity of suspended and saltating grains must therefore be higher for larger grain sizes, causing a stronger transverse bed slope effect. This is supported by the data in Figure 5, where a difference of a factor of 2 is observed between D_{50}=90μm (run 2), and 160μm (run 4&5) (Talmon, 1992).

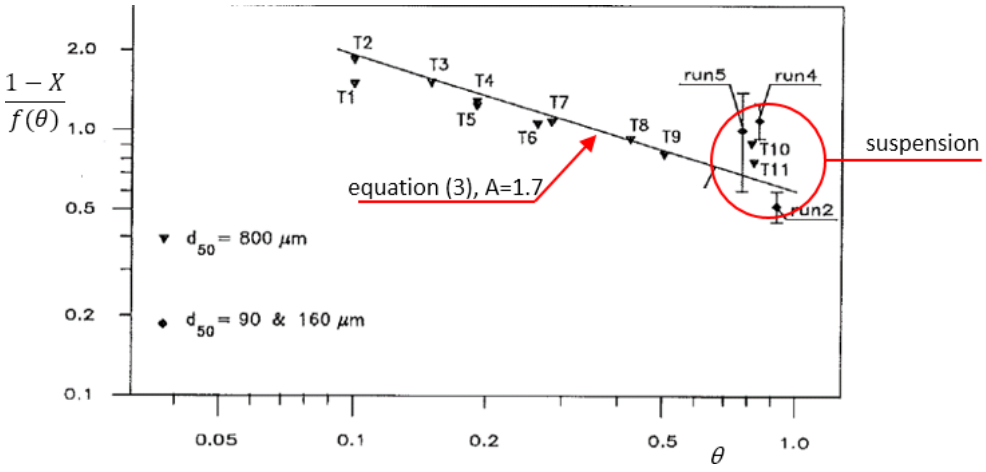

Figure 5, transverse slope effect for bed load and suspended load experiments (Talmon et al., 1995). X is the suspended load fraction. So the y-axis shows the transverse slope effect on bed load sediment only while for some experiments suspended load is also present.

1.2.6 Grain size, bed form type, and bed form scale

From experimental data it became evident that the transverse slope parameter $\frac{1}{f(\theta)}$ changes with different grain sizes. Differences occur in both A and the exponent of equation (4). A larger grain size leads to a decrease in $\frac{1}{f(\theta)}$ (Wiesemann et al., 2006). When transported as bed load, coarser grains travel at a larger vertical distance from the bed than finer material, as travelling height scales with grain size times two (Ashida & Michiue, 1972). The flow is also different, flow above coarse grains is hydraulically rough, whereas flow above fine grains is smooth (van Rijn, 2011, chapter 6). Depending on the exact shape of the logarithmic flow velocity profile fine grains may be transported in the laminar sublayer, while coarser grains may be transported in the buffer region above the laminar sublayer. The flow velocity in the laminar sublayer is lower than in the buffer region, therefore finer sediment will be transported in a region with a lower flow velocity than coarse sediment under the same hydrological conditions. Besides its effect on the type of flow, grain size is also a deciding factor for bed form stability together with Shields' number (Van den Berg and Van Gelder, 1993). Fine sediment tends to form ripples, whereas coarser sediment tends to form dunes under the same Shields numbers. The formation of ripples and dunes is caused by eddies in turbulent flow (van Rijn, 1984). For large grain sizes, large scale eddies responsible for the formation of dunes are already present at the beginning of motion, so the ripple stage is skipped.

Bed forms have a large effect on the transverse slope effect. Experimental data showed that for the same grain size the transition from a 3d ripple bed to a dune regime caused a decrease in $\frac{1}{f(\theta)}$ (Wiesemann et al., 2006). The size of bed forms also influences the bed slope effect. Satisfactory results for natural rivers were obtained after A in equation (5) was reduced with a factor two compared to A based on bed levelling experiments in a straight flume (Talmon et al., 1995). This was attributed to the differences in relative bed form scales between flumes and natural rivers. Bed forms in flumes are relatively large

compared to natural rivers due to scale differences. Bed form dimensions scale with grain size and water depth (Van Rijn, 1984):

$$\frac{\Delta}{h} \propto \left(\frac{D_{50}}{h}\right)^{0.3} \tag{9}$$

where Δ is dune height (m). A small water depth leads to small dunes which are relatively large compared to the water depth, and a large water depth leads to large dunes which are relatively small compared to the water depth. Including the van Rijn equations for relative bed form dimensions in equation (5) leads to the equation for the transverse slope effect in natural rivers (Talmon et al., 1995), which is currently most commonly used in morphological modelling:

$$f\left(\theta, \frac{D_{50}}{h}\right) = 9\left(\frac{D_{50}}{h}\right)^{0.3} \sqrt{\theta} \tag{10}$$

1.2.7 Inventory of data and transverse slope predictors

As seen in the previous sections of this literature review, there are currently many transverse slope predictors which are derived from research on different parameters and can be used in different situations. Table 1, on the next page, shows some well-known transverse slope predictors. Information is given on what data they were derived from and on which situations they are applicable.

Differences between the mentioned relations is large, a factor 10 difference in f(θ) exists between these equations for the same Shields number. Most have a dependence of the transverse slope effect to the inverse square root of Shields' number, combined with an empirically determined multiplication factor. They are either derived from experimental data or from a mathematical model which is tested against experimental data. The transverse slope effect can be derived from bed levelling experiments in straight flumes, where the rate at which a transversely sloped bed is relaxed to a horizontal state by the bed slope effect is measured (e.g. Talmon et al., 1995). With curved and carousels, the bed slope effect is derived from the equilibrium bed slope and a calculated angle between mean flow and secondary flow (e.g. Engelund, 1975). With mathematical models, a detailed force balance of a single grain on a sloping bed is considered which is then averaged over a high number of grains. A transverse slope effect model is then derived from this force balance and compared with experimental data (e.g. Sekine and Parker, 1992).

Table 1, some well-known transverse slope predictors.

Paper	Equation	Derived from	Applicable to
Talmon et al., 1995	$\tan(\alpha) = -\frac{1}{9\left(\frac{D_{50}}{h}\right)^{0.3}\sqrt{\theta}}\frac{\partial z_b}{\partial y}$	Bed levelling experiments in a straight flume and in the straight section of a curved flume. Bed load (D_{50}=0.785mm) & suspended load (D_{50}=0.09 & 0.160mm) experiments. Nondimensional sediment transport 0.1<θ<1.0.	Bed load transport & saltation on transverse slopes. Equation does not apply for suspended load.
Sekine & Parker, 1992	$\tan(\alpha) = -0.75\left(\frac{\theta_{cr}}{\theta}\right)^{\frac{1}{4}}\frac{\partial z_b}{\partial y}$	Mathematical modelling of saltating particles on a transverse slope. Tested against experimental data with water and air, 4°<α<32°, D_{50}=0.425, 0.7, 0.83 & 1.3mm.	Saltation and bed load transport on transverse slopes. There is an upper limit to θ beyond which particles collide, a value is not given. Small transverse angle α beyond which linear dependence between transport and transverse slope is lost.
Talmon & Wiesemann, 2006	$\tan(\alpha) = -c\frac{1}{\mu_c}\sqrt{\frac{\theta_0}{\theta_{eff}}}\frac{\partial z_b}{\partial y}$ Ripples: C=1, θ_{eff}=0.2θ'. Dunes: C=1.05, $\theta_{eff}=\theta'_{top}$.	Mathematical modelling of transverse slope effects for different grain sizes and bedforms. Tested against data from bed levelling experiments with straight flumes / straight part of curved flume in Delft and Darmstadt. D_{50}=0.09, 0.16, 0.78 & 0.96mm. 0.1<θ<0.9.	Bed load transport on transverse slopes. Can be used for a variety of grain sizes in the ripple and dune regime.
Wiesemann et al., 2006	Fine sand, ripples: $\tan(\alpha) = -\frac{1}{\sqrt{\theta}}\frac{\partial z_b}{\partial y}$ Coarse sand, dunes: $\tan(\alpha) = -0.9\frac{\partial z_b}{\partial y}$	Bed levelling experiments in a straight flume. D_{50}=0.25mm & 0.96mm. 0.1<θ<0.6. $n_{experiments}$~10 per grain size.	Bed load transport on transverse slopes. Fine sand, ripples is only applicable for 0.16<θ<0.5, beyond which dunes form.
Parker et al., 2003	$\tan(\alpha) = -0.7\sqrt{\frac{\theta_{cr}}{\theta}}\frac{\partial z_b}{\partial y}$	Mathematical modelling of bed load transport at low Shields stresses using a new equation for sediment entrainment on sloping beds.	Low Shields stresses, rolling particles. Slopes in arbitrary direction up to 22°.
Engelund, 1974	$\tan(\alpha) = -\frac{1}{\tan(30)}\frac{\partial z_b}{\partial y}$	Mathematical modelling of an equilibrium bed in a long circular bend.	Can be used to give a first approximation of bottom geometry of an endless circular bend with fixed walls.
Engelund, 1981 (in Mewis and Wiesemann, 2008)	$\tan(\alpha) = -\frac{1}{1.6\sqrt{\theta}}\frac{\partial z_b}{\partial y}$	Mathematical modelling of the force balance on a grain on a sloping bed.	Same as Engelund, 1974.
Ikeda, 1982 (modified by Parker, 1984)	$\tan(\alpha) = -\frac{1+\mu r}{\mu}\sqrt{\frac{\theta_{cr}}{\theta}}\frac{\partial z_b}{\partial y}$	Bed levelling experiments using air and water as transport medium. Three grain sizes were used for wind experiments. D_{50}=1.3mm was used for water experiments.	Bed load transport on transverse slopes.

1.2.8 Missing data and uncertainties introduced with bed levelling experiments

There is currently a lack of data. For each of the transverse bed slope predictors above, the number of experiments on which it is based is in the order of 5 to 20 per grain size. Data on grain sizes larger than 1.3mm is non-existent or inconclusive due to large scatter, and data for suspended sediment transport is scarce and not incorporated in current equations.

Most of the existing data is obtained from bed levelling experiments in straight (parts of) flumes. The following issues are inherent to this type of experimental setup: As the timescale of dune formation is similar to that of bed levelling, dunes are manually added to the bed at the beginning of each experiment (Talmon et al., 1995). The results are therefore largely influenced by the initial setup. Due to the manual preparation of bed forms its effect on the transverse slope effect cannot be adequately researched, and therefore is currently not accounted for in models. Secondly, the effect of helical flow is ignored whereas helical flows do occur even in straight flumes. This leads to the under-prediction of the transverse slope effect, as helical flow will increase the rate at which the bed is levelled. Thirdly, dunes adapt to the boundary conditions at the ends of the flume, which means that only the middle section provides useable data. Also the roughness changes during the bed levelling experiment as dunes adapt to flow conditions, leading to changes in sediment transport causing a difference between the amount of sediment fed into the flume and transported out.

Because of the uncertainties related to bed levelling experiments, the presence of multiple empirical factors in current transverse slope predictors, and large effect these have on model results (Schuurman et al., 2013) a tendency exists to use the transverse slope effect as a tool to calibrate model results to existing morphology (Talmon and Wiesemann, 2006; Wiesemann et al., 2006), ignoring important physical processes. For these reasons the transverse slope effect is currently the limiting factor in morphological modelling (Schuurman and Kleinhans, 2013).

1.2.9 Transverse slope effect in a carousel

In this research, experimental data will be collected using a carousel of which both the lid and floor can be rotated independently. In a carousel, a transverse slope is formed by helical flow instead of relaxed to a flat bed. Transversely sloping beds in carousels have been previously investigated (Engelund, 1975). Helical flows are strong in carousels and can therefore not be neglected as is done in bed levelling experiments. Due to this added complexity it has been proposed that only bed levelling experiments in straight channels provide useable data (Talmon and Wiesemann, 2006). But in fact, a simple helical flow predictor with the form of equation (6) can be used to reasonably predict transverse slopes in a carousel (Engelund, 1975). Moreover, the issues described in the previous section are not present in carousels. The presence of helical flow allows for the self-formation of a transverse slope, providing the possibility to measure a morphological equilibrium instead of measuring the rate of change of a disequilibrium. Experiments can be initiated with a flat bed, removing influence on the results of the initial setup and allowing the assessment of the effect of bed forms on the transverse slope effect.

The ability to rotate the carousel floor independently to the lid rotation provides the possibility to change the intensity of secondary flow. Secondary flow intensity depends on flow velocity, which is determined by both lid and floor rotation rate (Booij, 1994):

$$u_{av} = \omega_{lid} r \frac{1}{1+\sqrt{\Gamma}} + \omega_{floor} r \frac{\sqrt{\Gamma}}{1+\sqrt{\Gamma}} \quad (11)$$

where u_{av} is the average flow velocity (m/s), ω_{lid} and ω_{floor} are the rotation rates of the lid and floor (rad/s), and Γ is the ratio of the flume perimeter and its width ($\Gamma = \frac{w+2h}{w}$). Shear stress is determined by the flow velocity relative to the bed:

$$u_{av,r} = u_{av} - (\omega_{floor} r) \quad (12)$$

where $u_{av,r}$ is the average flow velocity relative to the bed. When the floor is counter rotated with a constant lid rotation rate, u_{av} is decreased. Meanwhile $u_{av,r}$ and shear stress are increased. This results in a weaker helical flow intensity. Optimal ratios between lid and floor rotation where secondary flow is reduced to near zero have been found (Booij, 1994). For these ratios u_{av} is near zero, while $u_{av,r}$ is approximately similar to the floor counter rotation rate, so that an endless straight channel is simulated. With co-rotation, u_{av} is increased, while $u_{av,r}$ is decreased, resulting in a stronger secondary flow intensity. A second helical flow cell may form when the absolute rotational velocities of both the lid and floor are larger than the average flow velocity (Booij, 1994; Figure 6), resulting in the reversal of the flow direction near the bed and direction of the transverse slope. These attributes provide the possibility to collect experimental data for a wide range of helical flow intensities and different helical flow directions, which means the influence of helical flow on the transverse slope effect can be assessed.

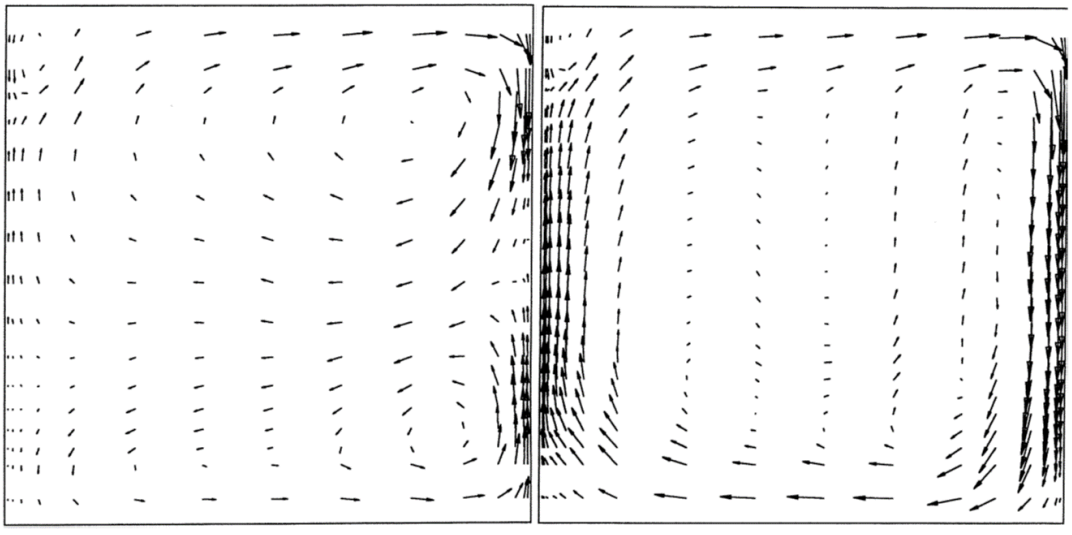

Figure 6, A: multiple secondary flow cells *B: single secondary flow cell*

1.3 RESEARCH QUESTIONS, OBJECTIVES, AND HYPOTHESES

1.3.1 Research questions

Due to the experimental setups in previous research it has not been possible to assess the transverse slope effect for a multitude of secondary flow intensities. The ability to change the intensity of helical flow allows to answer the following research question:

1. What is the effect of a transversely sloping bed on the mean direction of bed load transport in infinite bends with a range of helical flow intensities from near zero for optimal floor/lid rotation ratios to extreme helical flow intensities with floor co-rotation?

Because bed forms had to be pre formed by hand in bed levelling experiments, their influence on the transverse slope effect could not be isolated. The experiments of this research are initiated with a flat bed, allowing self-formation of bed forms and transverse slopes. Also, both 1mm and 4mm grains will be tested. This allows the following research questions to be answered:

2. How do bed forms influence the transverse slope effect?
3. And what is the effect of grain size?

As the flume has a circular shape, centrifugal forces will be present on both water and sediment:

4. What is the effect of centrifugal forces on flow and sediment transport?

Based on the new experimental data a transverse slope predictor will be derived. It will be compared with previous transverse slope predictors through bar modelling:

5. What are the implications of a transverse slope model based on experimental data from a carousel on bar modelling?

1.3.2 Objectives

Based on the literature review and research questions, the objectives of this study are to:

1. Create a larger and more comprehensive dataset of sediment transport on transverse slopes with coarse sand and gravel using experimental data from a carousel.
2. Derive a transverse slope predictor in the form of equation (4), in other words find a new f(θ), based on the new experimental data.
3. Assess the effect of the new transverse slope model on bar pattern modelling.

1.3.3 Hypotheses

Based on literature the following hypotheses are made:

1. In the case of an endless bend, the transverse slope that is formed is the result of the balance between upslope transport by helical flow and downslope transport by gravity.

2. The effect of bed forms is currently mostly unknown. In previous research (Wiesemann, 2006; Talmon and Wiesemann, 2006) the effect of bed forms has not been isolated from the effect of grain size, though according to the experimental data used in these studies the transverse slope effect under the dune regime is not dependent on Shields' number.
3. The transverse slope effect is known to be stronger for smaller grain sizes at similar Shields numbers (Wiesemann, 2006). This is likely related to the fact that the amount of sediment transport by flow is lower for smaller grains at the same Shields numbers. Leading to a perceived stronger slope effect as it has an inverse proportionality to Shields' number and sediment transport.
4. Centrifugal force on water generates secondary flow. Centrifugal force is both present on sediment located on the bed and sediment that is being transported. Centrifugal force on the bed will cause the bed to collapse slightly, reducing the transverse slope's steepness. Centrifugal force on moving sediment will push the sediment towards the outer bend. For both cases, the observed transverse slope effect will be perceived as stronger.
5. The new transverse slope model is expected to give more realistic results, as the experimental data is derived from a wider range of flow and transport conditions than datasets on which previous transverse slope effect predictors are based.

2 MATERIALS & METHODS

2.1 EXPERIMENTAL SETUP

Experimental data was collected in the Cees Kranenburg carousel located in the Water Lab of Delft University of Technology (Figure 7). The donut shaped flume has a circumference of 11.7m, a diameter of 3.7m, a width of 0.3m, and a height of 0.47m. The flow is driven by a rotating aluminium top lid. The floor can be rotated independently of the lid, by which the intensity of secondary flow can be manipulated. Sand is added up to a height of 15cm, and the edge of the top lid is set at a height of 36cm. This results in an average water depth of 21cm.

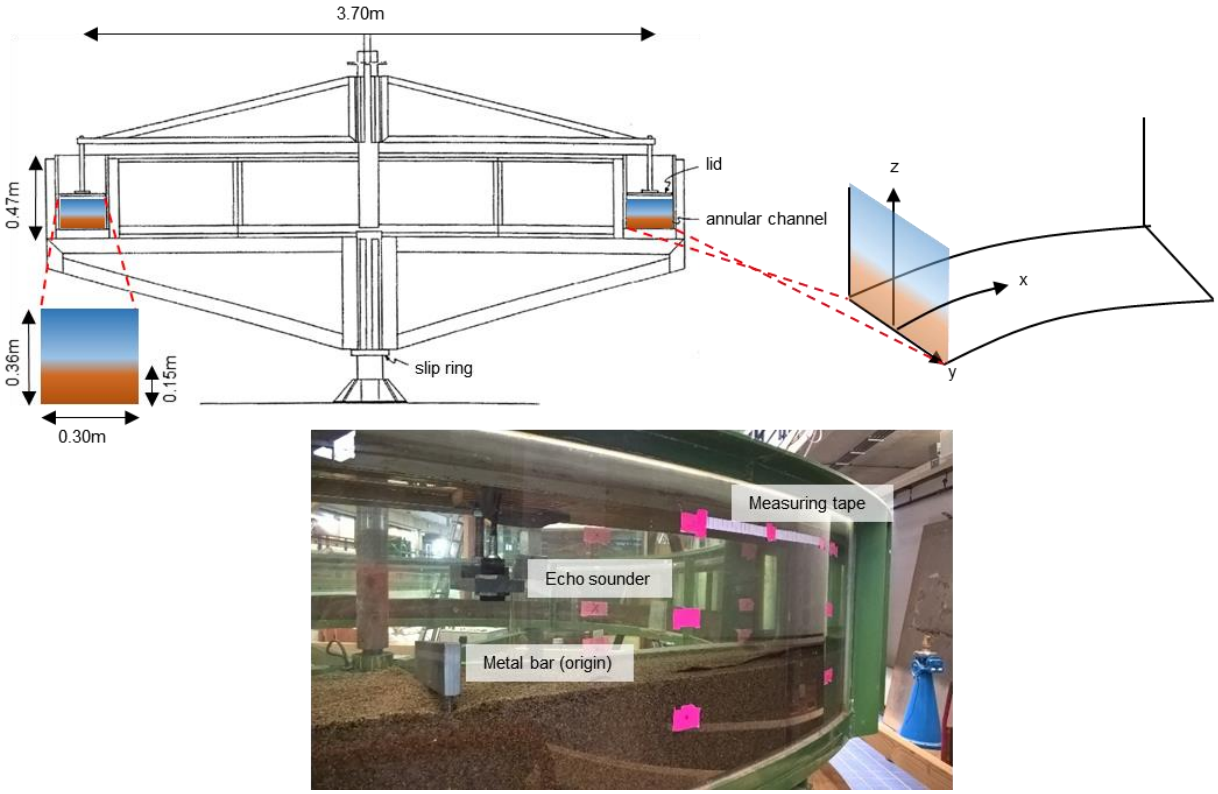

Figure 7, Schematic drawing of the experimental setup and the coordinate system, and a picture of the experimental setup with measuring equipment.

When morphological balance is reached, the rotation is stopped and bed elevation is measured. Water depth is measured along six horizontal transects with an echo sounder. The transects cover a width of 21.4cm. The echo sounder has a sampling rate of 10Hz and a polling rate of 1000Hz. It is moved over the bed with a velocity of approximately 0.2m/s, which results in a data point cloud with a density of 2 cm in the x-direction and 4.4 cm in the y-direction. Bed elevation is obtained from the measured water depth. As the carousel has no clear starting point, a metal bar is put on the bed during measurement to serve as an origin in the water depth data.

Two cameras are used for image capture during the experiments. A webcam is located next to the outer wall of the flume, and a second camera is attached to the inner wall. The webcam takes pictures at a set interval depending on the rotation velocity of the floor and rate of morphological change. The second camera provides video data of the first 30 minutes of each experiment. Both cameras are used to measure dune migration rate, which is used for calculation of sediment transport and Shields' number. The video camera provides dune migration data of experiments with high dune migration rates (>1cm/min), the webcam provides data of low dune migration rates.

2.2 DATA COLLECTION

Experiments were run in systematic series of flow and transport conditions. Separate series were run for 1mm and 4mm grains. These series are part of a larger dataset in which smaller grain sizes, grain size mixtures, and light sediment will be included (PhD research of A.W. Baar). For this research coarse uniform grains were chosen to avoid complex variables which are introduced with suspension and sediment sorting. The experimental series consist of various lid rotation rates between the beginning of motion and the maximum setting of the flume, and various floor rotation rates to include many secondary flow intensities. The step between lid rotation rates was 0.5 seconds per rotation for 4mm grains. A step of 1 second per rotation was chosen for 1mm grain as the range possible rotation rates was much larger due to the higher mobility of these grains. The hiatus between floor rotation rates was chosen as 10 seconds per rotation, and for each lid rotation rate a floor rotation rate was found for which the transverse slope remained horizontal. A ratio $\frac{\omega_{lid}}{\omega_{floor}}$ of -1.6 is expected to form a horizontal bed, as secondary flow velocity is minimal for this ratio (Booij, 1994). Systematically running these series results in a dataset with a high density of sediment mobility's and helical flow intensities. In Figure 8 the range sediment mobility and bed states covered by the experiments is shown in a bed form stability diagram (Van den Berg and Van Gelder, 1993). Indeed, dunes were present for all experiments with one exception, a lower stage plane bed formed during the slowest 1mm run.

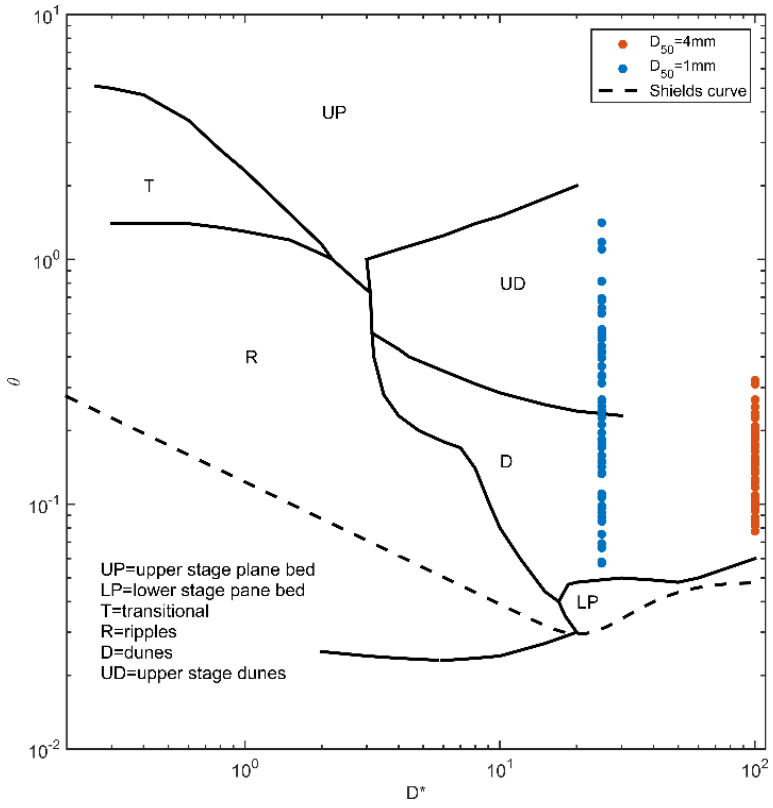

Figure 8, range of morphological conditions covered by the experiments plotted on the bed state stability diagram of Van den Berg and Van Gelder (1993).

2.3 DATA ANALYSIS

2.3.1 Sediment transport and Shields' number

Dune migration velocity is measured manually from observation of photo and video data. Sediment transport rate can then be calculated as:

$$q_b = u_{dune} * \Delta * (1 - \lambda) \qquad (13)$$

where u_{dune} is dune migration velocity (m/s), Δ is dune height (m), and λ is porosity. Well sorted sand is used in all experiments, therefore λ is taken as 0.4.

The total dune area is determined by averaging the total longitudinal dune area of all measured bed elevation transects and multiplying this number with the flume width of 0.3m. The longitudinal dune area is determined by calculating the area between the measured bed elevation and a line which connects the troughs (Figure 9). Dune height is obtained by dividing the measured area with the measurement length along the x-axis.

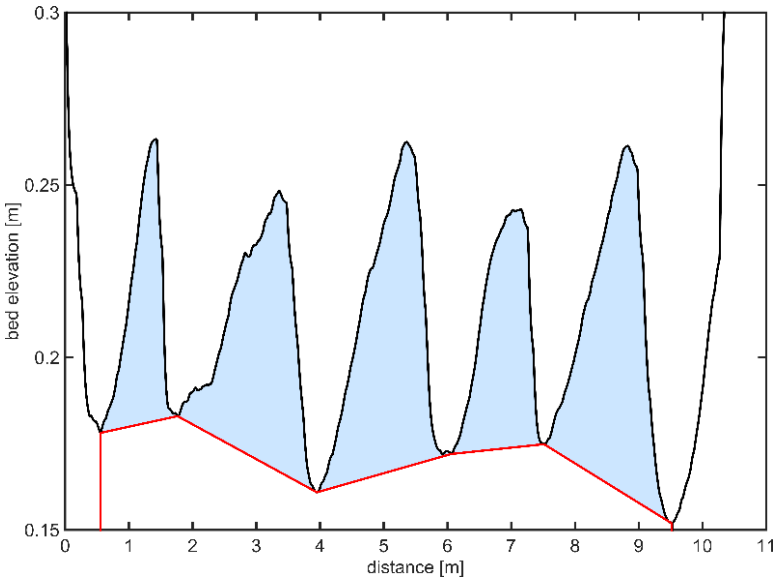

Figure 9, example of total dune area calculation on one transect.

Shields' number is back calculated from the measured sediment transport data by calibration of the Chézy roughness coefficient used in calculated sediment transport rates to measured sediment transport rates (see equations (2) and (3)). Bed load transport per unit width can be calculated as:

$$q_b = \phi_b * \sqrt{\frac{\rho_s - \rho_w}{\rho_w} g} * {D_{50}}^{\frac{3}{2}} \quad (14)$$

where φ_b is the Einstein number, which for bed load transport can be calculated by (Meyer-Peter and Mueller, 1948):

$$\varphi_b = \alpha(\theta - \theta_{cr})^{1.5} \quad (15)$$

where θ_{cr} is the critical Shields number for the initiation of sediment transport. It is calculated using the following equation, which is applicable for $0.05<D_{50}<5$mm (Kleinhans, 2005):

$$\theta_{cr} = \left(0.145 {Re_p}^{-\frac{1}{3}} + 0.045 * 10^{\left(-1100 {Re_p}^{-1.5}\right)}\right) \quad (16)$$

where Re_p is the particle Reynolds number:

$$Re_p = {D_{50}}^{1.5} \frac{\sqrt{\frac{\rho_s - \rho_w}{\rho_w g}}}{\nu} \quad (17)$$

where v is the viscosity of water, which is taken as $1 \cdot 10^{-6}$ for water at room temperature.

2.3.2 Secondary flow

The helical flow relation of Engelund, 1974 is used to predict the angle between the direction of shear stress and x, as it is derived from consideration of an endless bend. The angle is calculated from equation (6), where the helical flow factor β depends roughly on a ratio between the average tangential flow velocity u_{av} and the shear velocity. The average tangential flow velocity is calculated from equation (11). Shear velocity u* is calculated as:

$$u^* = \sqrt{\frac{\tau}{\rho_w}} \tag{18}$$

The helical flow coefficient β (see equation (6)) is calculated by:

$$\beta = h\frac{u_0}{\epsilon_0}\left(\frac{1}{2}\zeta^2(\alpha-1) + \frac{1}{6}B\zeta^4 - \frac{1}{30}B^2\zeta^6 + K\right) \tag{19}$$

where u_0 is the tangential flow velocity at the water surface, ϵ_0 is the eddy viscosity, ζ is the relative location along the z-axis ($\frac{z}{h}$, where z is the distance below the water surface), and α, B, and K are coefficients that depend on a ratio between shear velocity and depth averaged flow velocity. The eddy viscosity is a factor of the shear velocity and water depth:

$$\epsilon_0 = 0.077u^*h \tag{20}$$

The tangential flow velocity at the water table is be back-calculated from the average tangential flow velocity under the assumption that the 2-d flow velocity profile is approximately logarithmic (Van Rijn, 2011):

$$u_0 = \frac{u_{av}}{\frac{ks}{Ch} - 1 + \ln\left(C\frac{h}{ks}\right) * \ln\left(C\frac{h}{ks}\right)} \tag{21}$$

where ks is the Nikuradse roughness height ($2.5D_{50}$). The coefficient B from equation (19) is a factor of tangential flow velocity and shear velocity:

$$B = 6.5\frac{u^*}{u_{av}} \tag{22}$$

The other helical flow coefficients α and K are a function of B:

$$\alpha = \frac{1 - B + \frac{3}{5}B^2 - \frac{1}{7}B^3}{1 - \frac{1}{3}B} \tag{23}$$

$$K = \frac{1}{6}(1-\alpha) - \frac{1}{30}B + \frac{1}{210}B^2 \tag{24}$$

The shape of the ratio between helical and tangential flow is given in Figure 10. When flow velocity increases, the helical flow coefficient β changes very little, as it depends on the shape of the flow profile along the depth, which remains approximately similar with different depth averaged flow velocities. Therefore, while helical flow velocity increases with increasing depth averaged flow velocity, the angle between mean flow and helical flow hardly changes. The ratio between the shear stress direction and the x-axis on the grains is calculated at the distance z below the water surface for grains transported as bed load (Ashida & Michiue 1972):

$$z = h - (2 * D_{50}) \tag{25}$$

which gives a sediment transport height of respectively 2 and 8mm above the bed for 1 and 4mm grains. From the general shape of the ratio between helical and tangential flow it is observed that different transport heights do have an influence on this ratio. Helical flow is slightly stronger for larger grains.

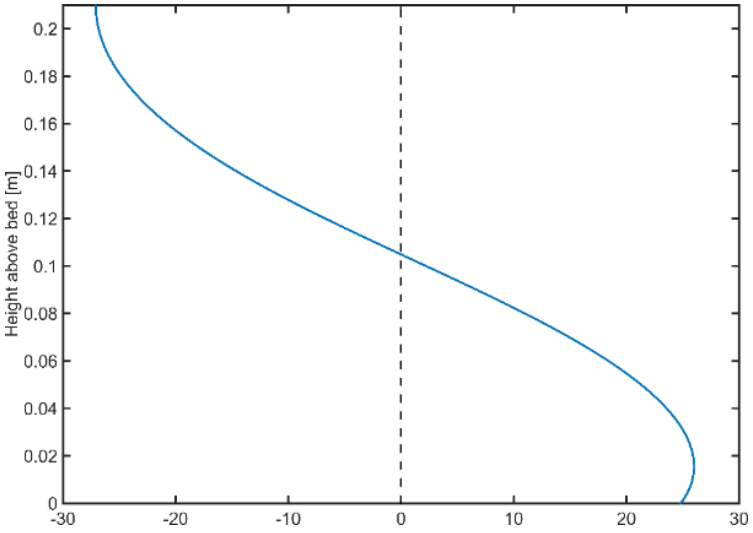

Figure 10, helical flow profile in the y-z plane as derived from Engelund, 1974.

When morphological balance is reached, the downslope angle of deflection of the shear stress vector from x due to the sloping bed is balanced by the upslope angle of helical flow so that $-\tan(\delta) = \tan(\alpha)$.

2.3.3 Centrifugal force on bed and sediment

Due to the ability to rotate the floor with this particular flume, sediment particles on the bed are subjected to a centrifugal force. Centrifugal force is related to the mass, rotational velocity, and bend radius as:

$$F_c = m\omega^2 r \tag{26}$$

where m is the mass of a single grain which can be calculated by multiplying its volume with its density under the assumption that their shape is approximately spherical.

A centrifugal force also acts on mobile grains which are not attached to the bed as they propagate in a curve. Equation (26) may also be applied for this case. Because the centrifugal force on these grains is not influenced by the rotational velocity of the floor, the travel velocity is approximated as (Bridge et al., 1984):

$$u_{grains} = a(u^* - u^*_{cr}) - (\omega_{floor} r) \quad (27)$$

where u_{grains} is the absolute velocity of the grains (m/s), u^*_{cr} is the critical shear velocity for the initiation of sediment transport, and a is an empirical factor calculated as:

$$a = 2.5 \log\left(\frac{D_{50}}{ks}\right)\left(2.53\sqrt{\theta - \theta_{cr}} + 0.5\right) + 8.5 \quad (28)$$

Outward centrifugal force can now be compared with inward drag force by helical flow. The inward drag force by helical flow can be determined by multiplication of the inward directed shear stress by helical flow (N/m^2) and the area of a grain:

$$F_{helical} = \tau_{helical} . A_{grains} \quad (29)$$

where $F_{helical}$ is the inward drag force from helical flow, τ_{helial} is the inward directed shear stress from helical flow which can be calculated from the angle between mean and secondary flow (section 2.3.2), and A_{grains} is the area of a grain determined from D_{50} under the assumption that grains are spherical.

2.3.4 Transverse slope

Bed elevation is measured along six horizontal transects with equal distance between them. The transverse slope effect is measured between transect 2 and transect 5, as the transverse slope is influenced by side wall effects. The mean bed elevation is determined for each of these transects, creating a mean bed profile in the y-z plane (Figure 11). Hereby the 3-d shape of the bed profile is averaged over the length of the flume, which means that the measured transverse slope is caused by balance between the transverse slope effect and length averaged helical flow, and is therefore applicable to equation (4). $\frac{\partial z_b}{\partial y}$ is taken as the average of the two steepest measured slopes between transect 2 and 5 to minimize influence of bed forms on the measured slope. The y and z coordinates of each measured slope used to determine local water depth and bend radius for the calculation of helical flow.

Each point in Figure 11 is the average of over 10^3 echo sounder measurements, therefore the measured transverse slope is very precise. The uncertainty of each data point can be assessed by dividing the standard deviation with the square root of the number of measurements. For the transverse slope measurements in this research the uncertainty was in the order of 1mm.

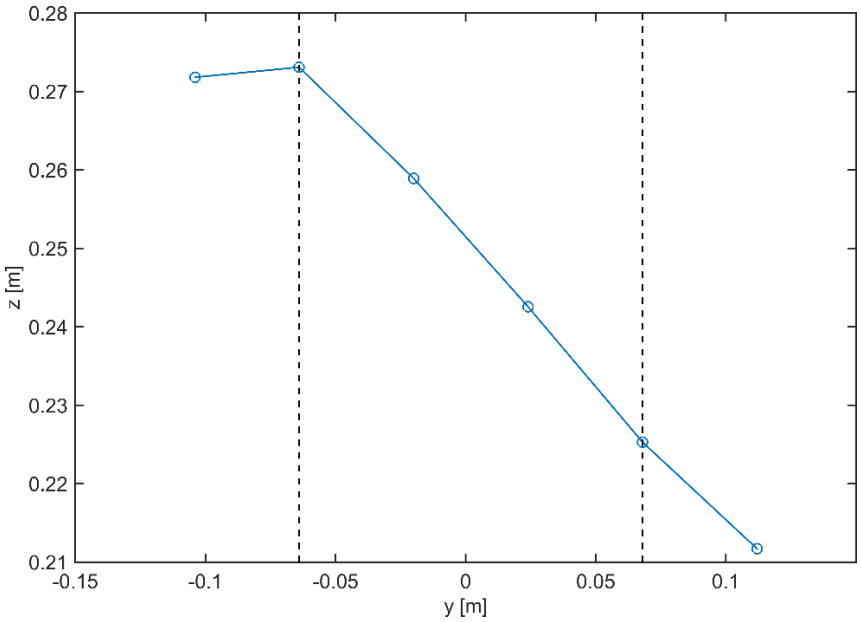

Figure 11, example of mean transverse bed elevation. The black lines indicate transect 2 and 5. y values are relative to the location of the average radius.

3 RESULTS

3.1 GENERAL OBSERVATIONS ON BED ELEVATION & TRANSVERSE SLOPE DATA

Figure 12 shows a series of bed elevation data for increasing counter and co-rotation of the floor with a set lid rotation rate. This illustrates the pattern in the transverse slope angle that is observed in all experiments. Table 2 shows the summary of important observations on flow and sediment transport direction. Dunes are present in almost all experiments, which is as expected according to Figure 8. When secondary flows are strong, the shape of the dunes is skewed. When secondary flow is directed inwards, dunes are relatively higher near the outer wall due to much deeper troughs than near the inner wall, but bed elevation at the dune heads is lower. This is illustrated by the mean bed elevation profiles on the right side of the figure. When moving from the innermost measurement (y=-0.1) to the outermost measurement (y=0.1) the bed mean bed elevation drops, but the distance between the minimum and maximum and the 25^{th} and 75^{th} percentiles is increased due to the increase in dune height. This pattern is reversed when secondary flow is directed outwards during experiments with high floor counter rotation rates.

When the floor is not rotated, a transverse slope is self-formed due to the balance between secondary flows carrying sediment upslope and gravity dragging sediment downslope as explained in sections 1.2.3 and 1.2.4. The steepest slope is usually observed near the centre of the flume. u_{av} is lower near the inner wall, as the radius of the bend is smaller while angular velocity remains equal. Secondly, side wall boundary effects reduce sediment transport by helical flow (see Figure 6). These effects are responsible for the slightly sinusoidal shape of the transverse slope.

Counter rotation of the floor leads to a change in Shields' number, degree of flow helicity, transverse slope, and change in bedform shape and size as expected from equations (11) and (12). The second example of bed elevation data in Figure 12 shows a case in which secondary flow is decreased by counter rotation of the flume's floor towards near zero causing the transverse bed profile to be flattened. Counter rotation of the floor increases Shields' number, as the entire bed is rotated against the flow. But u_{av} is decreased due to the drag force of both side walls and the bed in the opposite direction of flow velocity. This leads to a decrease in secondary flow velocity due to the decrease of centrifugal forces on the water, which in turn leads to a decrease in the transverse slope's angle. Compared to the bed profile of the first example in Figure 12, the dunes are smaller and the number of dunes is higher. The degree of variation in bed elevation along the longitudinal transects is decreased. Moreover, the amount of vertical and horizontal skewness of the dunes is less.

The third example of Figure 12 shows a case where a high counter rotation rate led to the reversal of the direction of the transverse slope. In this case bed form patterns are similar to the first example, only the patterns in the x-direction are opposite. The variation in bed elevation is high due to the high relative flow velocity $u_{av,r}$, forming larger bed forms. Centrifugal forces on the sediment are high due to the high radial

velocity of the bed. The reversed direction of the transverse slope may be caused by the presence of a second helical flow cell (Figure 6), or outward centrifugal forces being larger than the inward force by near zero helical flow. When counter rotation velocity of the floor is increased in small steps the inward directed transverse slope decreases gradually until it is zero, after which an outward directed slope is formed of which the steepness increases much faster.

The last example in Figure 12 is that of a co-rotation of the floor. In this case the helicity of the flow is increased compared to an experiment without floor rotation. The flow is both driven by the lid and the floor, increasing u_{av} and thus centrifugal forces on the water and helical flow. But as the floor is co-rotated, $U_{av,r}$ is decreased while the relative secondary flow velocity remains equal. This leads to an increase of upslope transport of sediment compared to transport in the x-direction, and therefore to an increase of the transverse slope's angle. A high amount of small dunes is observed in these experiments. It is also observed that the transverse slope does not propagate to the inner wall of the flume. The mean bed elevation at the innermost measured transect is equal to the initial bed elevation at the start of the experiment, which means that in this case little to no sediment transport is present here.

Table 2, Short summary of observations on flow and sediment transport (direction) as described in this section. $\frac{\partial z_b}{\partial y} < 0$ *is a transverse slope directed towards the inner bend.*

Experiment	Observations
No counter rotation ($\frac{\partial z_b}{\partial y} < 0$)	• Control case on which other observations are based

Counter rotation ($\frac{\partial z_b}{\partial y} \cong 0$)	• Relative flow velocity +
	  ○ Sediment transport +
	• Absolute flow velocity –
	  ○ Helical flow velocity -
	• Centrifugal force +

Counter rotation ($\frac{\partial z_b}{\partial y} > 0$)	• Relative flow velocity ++
	  ○ Sediment transport ++
	• Absolute flow velocity –
	  ○ Helical flow velocity –
	• Centrifugal force ++

Co-rotation ($\frac{\partial z_b}{\partial y} < 0$)	• Relative flow velocity –
	  ○ Sediment transport –
	• Absolute flow velocity +
	  ○ Helical flow velocity +
	• Centrifugal force +

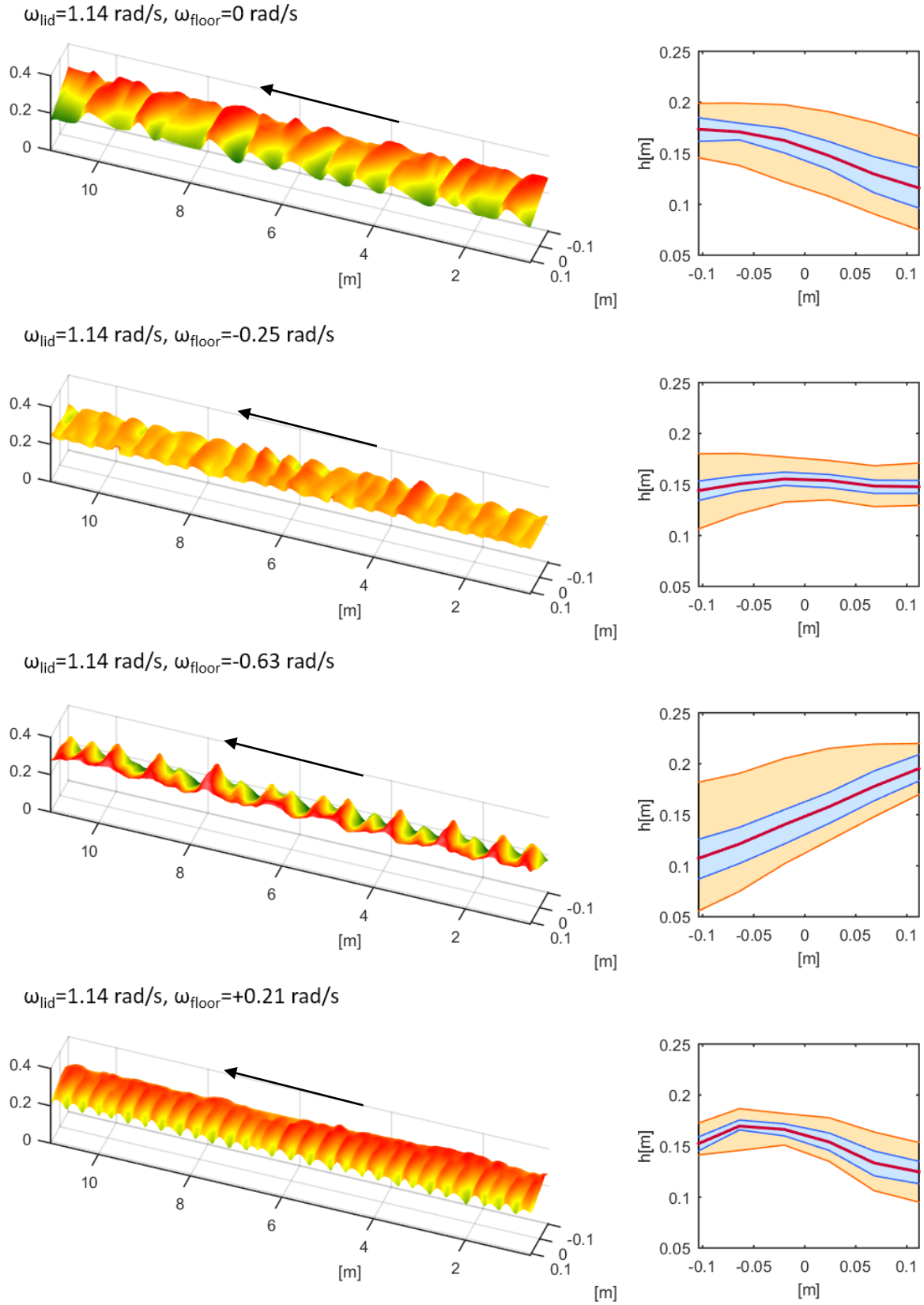

Figure 12, example of a series with increasing counter and co-rotation rate for a single lid rotation velocity. On the left side is the bed profile and on the right side is the mean bed elevation profile in the y-z plane. The arrows indicate flow direction. The red line indicates mean bed elevation, the orange lines the minimum and maximum, and the blue lines the 25th and 75th percentiles.

3.2 CALCULATION OF FLOW VELOCITY AND SHIELDS' NUMBER

Sediment transport rate was measured from dune migration rate as described in section 2.3.1. Figure 13 shows the results of the back calculation of and correction on flow velocity and Shields' number. A calibration was performed on the Chézy roughness coefficient and critical Shields number. A good fit was found for C=36.4 $m^{1/2}/s$ in combination with θ_{cr}=0.05 for 1mm grains and θ_{cr}=0.08 for 4mm grains. The spread in data of 1mm sediment is high due to the occurrence of saltation while bed load transport equations are used, and a higher error in dune migration measurement due to turbidity of the water. While equation (11) is derived from consideration of a flume without sediment, a good correlation exists with flow velocities which were back calculated from sediment transport (Figure 13 C). Therefore equation (11) is found to provide a good estimation of the flow velocity for experiments where sediment transport rates could not be measured.

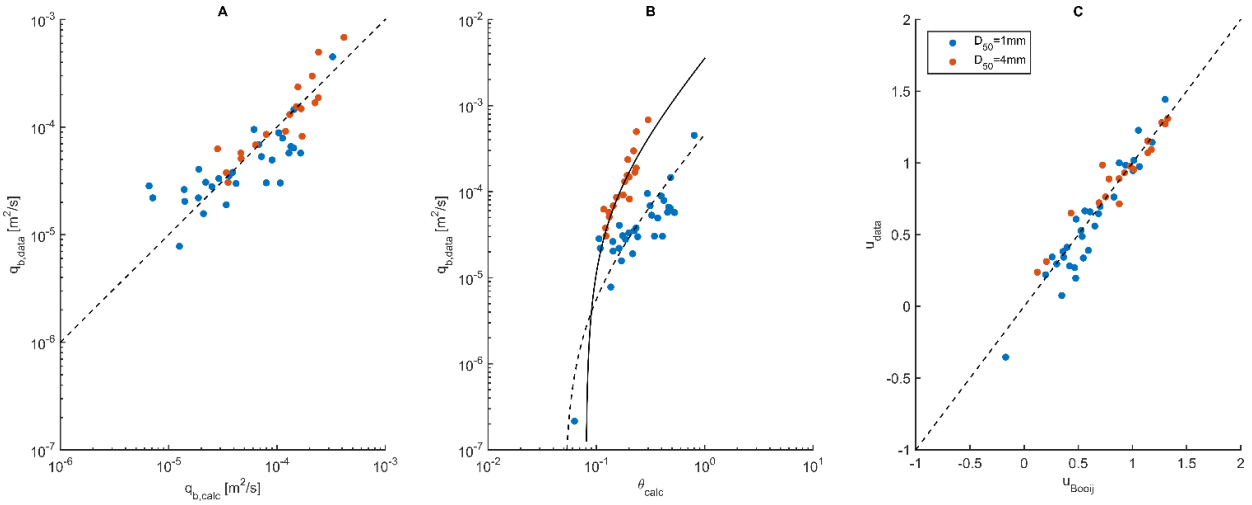

Figure 13, A: measured against calculated sediment transport. B: measured sediment transport against calculated Shields' number. C: flow velocity calculated from equation (11) against flow velocity back calculated from transport.

3.3 TRANSVERSE SLOPES WITH LID ROTATION ONLY

Rotation of only the top lid includes smallest number of variables which is possible in this experimental setup. The results of these experiments are given in Figure 14.Because the floor is not rotated centrifugal forces on the bed are zero. The angle between the shear stress vector and the x-axis varies very little over θ, as the ratio between u_{av} and u* remains approximately equal (section 2.3.2; Figure 14 C). Helical flow is stronger for 4mm grains. This is explained by the difference in travelling height between 1mm and 4mm grains. As bed load, 1mm grains travel at a height of approximately 2mm, and 4mm grains travel at roughly 8mm above the bed. Consequently, ζ in equation (19) is smaller for 4mm grains, which leads to an increase in the helical flow coefficient β, and thus a larger angle between shear stress and the x-axis. Secondly, the shape of the logarithmic flow velocity profile differs with grain size. Due to the influence of grain size on ks, u_0 is larger for 4mm grains, which also leads to an increase of β. Figure 14 B shows the change in steepness of the transverse slope for increasing Shields' numbers. As Shields' number increases, the transverse slope

increases. This is caused by the increase in net upslope transport due to helical flow. Grain size does not have influence on the transverse slope effect when Shields' numbers are normalized by dividing them with θ_{cr} (0.05 and 0.08 for 1 and 4mm grains respectively). An exponential increase of $\frac{\partial z_b}{\partial y}$ is observed for 4mm sediment as shown by the straight line on a log scale in Figure 14 B. The same pattern is observed with 1mm sediment from the beginning of motion up to $\theta/\theta_{cr} \approx 2.5$. Hereafter the steepness of the transverse slope rapidly drops and proceeds to increase at a slower rate.

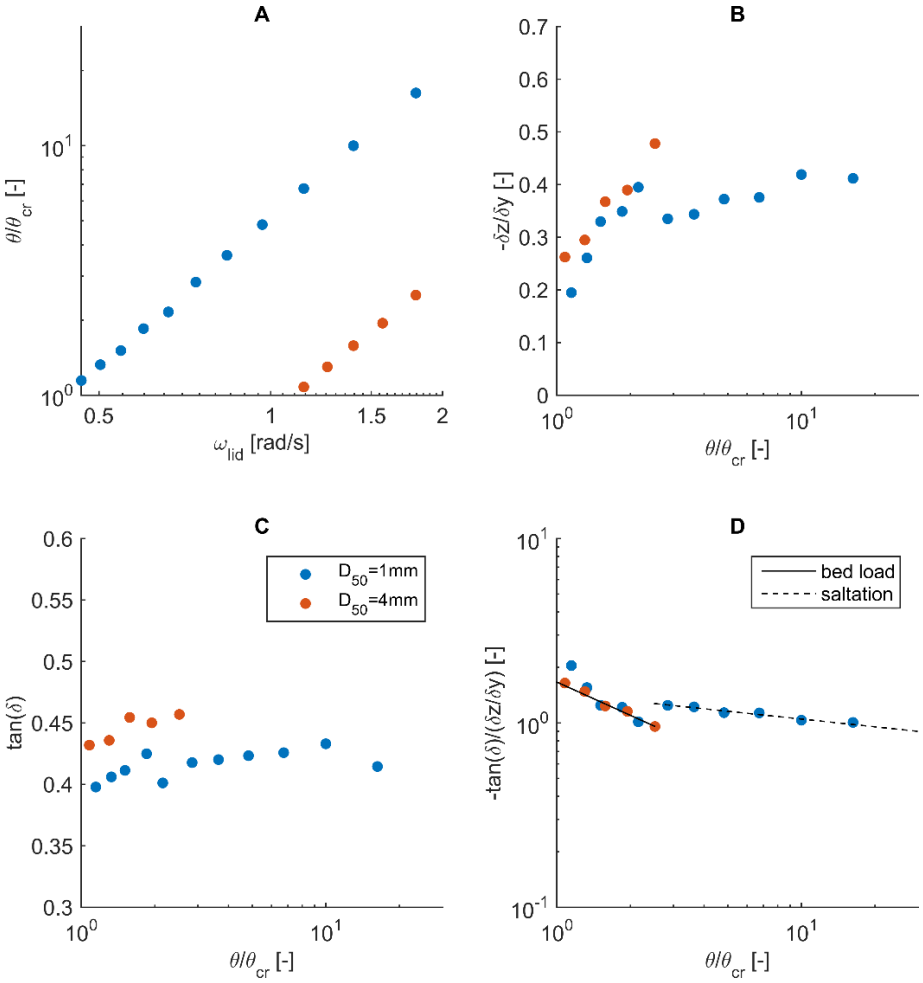

Figure 14, A: θ/θ_{cr} against lid rotation rate. B: increase of transverse slope with increasing θ/θ_{cr}. C: change of helical flow intensity against θ/θ_{cr}. D: transverse slope effect for lid rotation only.

The transverse slope effect is shown in Figure 14 D. The transverse slope effect is indeed inversely proportional to Shields' number as expected from equation (4). When taking in account that tan(δ) changes little over θ, it is observed that the transverse slope effect becomes weaker when Shields' number is increased. At $\theta/\theta_{cr} \approx 2.5$ the mode of transport is observed to change from rolling to saltation. When sediment is saltating, the increase of the transverse slope is slowed down. This implies that the transverse slope effect for saltation is stronger than that of bed load transport, which is indeed observed in Figure 14 D. In

the calculation of the transverse slope effect a discrimination must therefore be made between different transport modes. For rolling (up to $\theta/\theta_{cr}<2.5$), the transverse slope effect may be calculated by:

$$f(\theta)_{bed\ load} = 0.60\left(\frac{\theta}{\theta_{cr}}\right)^{0.6} \quad (30)$$

And:

$$\tan(\alpha) = -1.67\left(\frac{\theta_{cr}}{\theta}\right)^{0.6}\frac{\partial z_b}{\partial y} \quad (31)$$

And for saltation ($\theta/\theta_{cr}>2.5$):

$$f(\theta)_{saltation} = 0.69\left(\frac{\theta}{\theta_{cr}}\right)^{0.14} \quad (32)$$

And:

$$\tan(\alpha) = -1.45\left(\frac{\theta_{cr}}{\theta}\right)^{0.14}\frac{\partial z_b}{\partial y} \quad (33)$$

R^2 values are 0.82 for rolling and 0.97 for saltation.

3.4 TRANSVERSE SLOPES WITH FLOOR ROTATION INCLUDED

3.4.1 Centrifugal forces on bed and sediment

The flattening and reversal of direction of the transverse slope can be caused by the presence of a second helical flow cell, or it can be caused by outward centrifugal force exceeding the inward shear force by helical flow when it is reduced to near zero. To test this the magnitude of the centrifugal force is compared against the inward force from shear stress exerted by helical flow. A comparison is shown for grains which are mobile, and grains located on the bed (Figure 15). While a relation is visible between increasing centrifugal forces and the decrease and reversal of the transverse slope, centrifugal forces on a single grain are at least a factor 1000 smaller than the inward force by shear stress for both mobile grains and grains located on the bed and are therefore considered negligible. The change in transverse slope must therefore be solely caused by the change in angle between shear stresses due to the change in relative helical flow as described earlier.

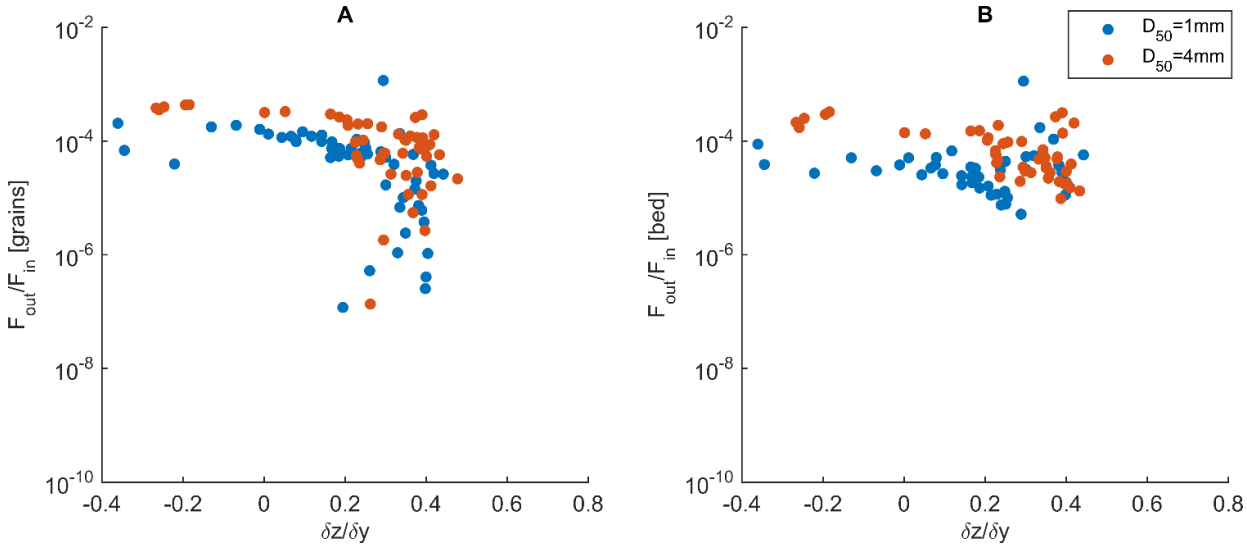

Figure 15, A: force balance for moving grains against transverse slope. B: force balance for grains located on the bed against transverse slope.

3.4.2 Presence of a second helical flow cell

The only mechanism that allows the reversal of the direction of the transverse slope with high floor rotation rates is the presence of a second helical flow cell as it cannot be explained by centrifugal forces. This second cell may be present when the rotational velocities of both the lid and floor are higher than u_{av}. When flow near the floor is higher than u_{av} the change in centrifugal force on the water over the z-axis responsible for helical flow is reversed between the depth at which $u=u_{av}$ and the floor. The flow near the floor is then driven outwards forming another helical flow cell which flows in the opposite direction compared to normal helical flow.

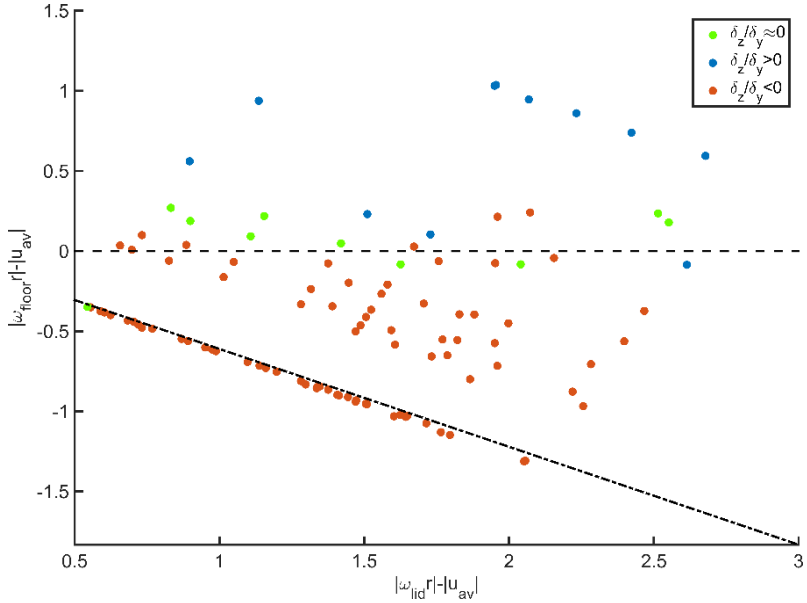

Figure 16, presence of two secondary flow cells (above the horizontal line) according to Booij, 1994 and the direction of the transverse slope.

Figure 16 shows the direction of the transverse slope's angle and the amount of secondary circulation cells according to the theory of Booij, 1994. Below the horizontal line one circulation cell is present, which should lead to an inward transverse slope. Above the horizontal line two cells are present which should lead to an outward directed transverse slope. -0.05<$\frac{\partial z_b}{\partial y}$<0.05 is considered as near horizontal. Indeed, two secondary flow cells are present for all but one reversed transverse slope and near horizontal beds are present around the beginning of the formation of a second cell. A clear distinction is visible between experiments with floor counter rotation and experiments where ω_{floor}=≤0 rad/s. The latter are all plotted on a single line, of which the slope is equal to the increase of flow velocity with increasing co rotation rate. According to equation (11) this slope is equal to $-\frac{\sqrt{\Gamma}}{1+\sqrt{\Gamma}}$, which in this case is approximately -0.6. A second helical flow cell cannot form under situation with floor co rotation. The floor's rotational velocity may only exceed u_{av} when u_{av} exceeds the lid's rotational velocity, therefore the conditions for the presence of a second cell cannot be met.

3.4.3 Transverse bed slopes

Figure 17 shows the change of the transverse slope's angle for different ratios between lid and floor rotation rates. Steep transverse slopes directed towards the inner bend are present for positive $\omega_{lid}/\omega_{floor}$ ratios. For floor counter rotation, the transverse slope's angle decreases with decreasing $\omega_{lid}/\omega_{floor}$ ratio and eventually switches direction. This is in agreement with the observations in section 3.1 and the considerations on flow and transverse slopes in carousels of section 1.2.9. The vertical scatter in Figure 17 is caused different helical flow velocities with the same $\omega_{lid}/\omega_{floor}$ ratio, as u_{av} is an independent variable in this figure.

According to the equations in section 2.3.2 the absolute secondary flow velocity may only be reduced to zero when the absolute tangential flow velocity is zero, which is at $\omega_{lid}/\omega_{floor}$=-1.8 according to equation (11). But it is observed that the transverse slope flattens at higher ratios, where the tangential flow velocity is nonzero and helical flow does occur. Moreover, different transverse slope angles are observed for the same $\omega_{lid}/\omega_{floor}$ ratio of flattened transverse slopes. This implies that the presence of sediment and bed forms causes differences between the actual flow velocity and the flow velocity calculated using equation (11), especially when flow velocity is near zero.

A reversal of the direction of the transverse slope is observed for high counter rotation rates which was also observed in section 3.1. The change in direction and increase in the reversed transverse slope's angle is very rapid compared to the initial decrease of the slope when counter rotation is increased. Steep transverse slopes in reverse direction are observed while δ is near zero according to the theory of Engelund, 1974, which means that 1D helical flow calculation cannot be used for cases with multiple secondary flow cells.

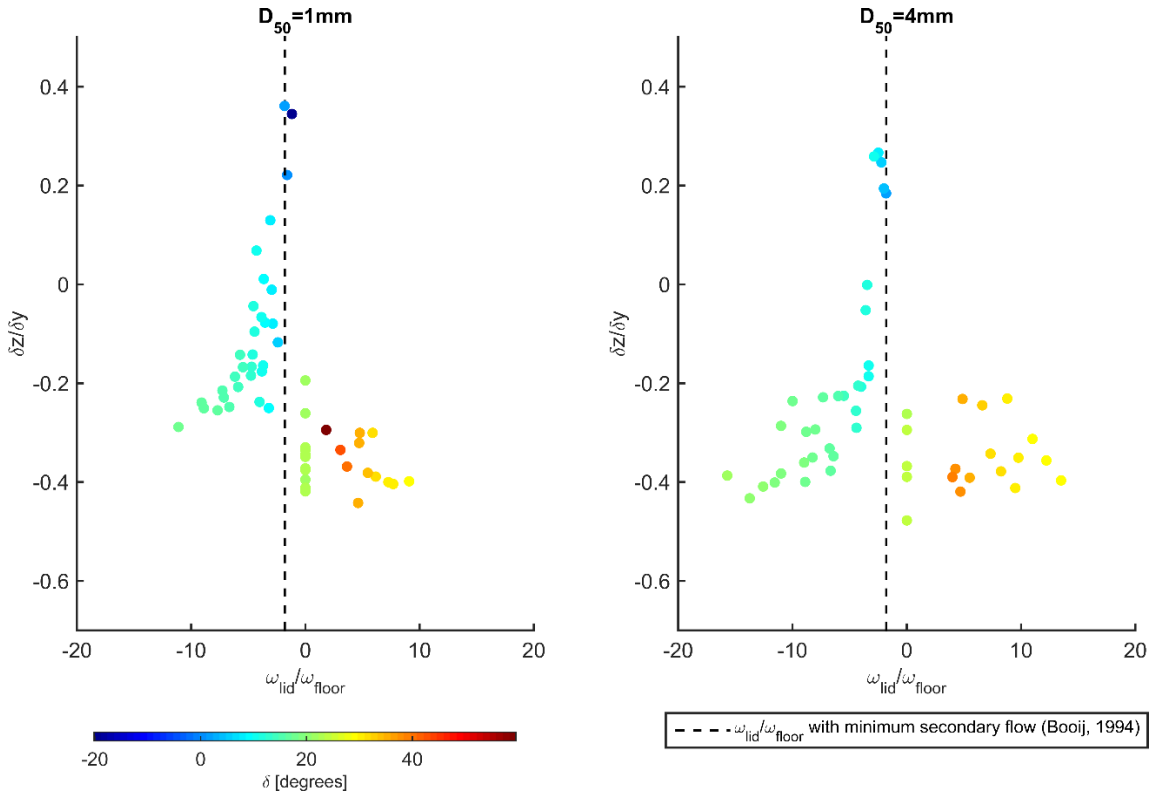

Figure 17, transverse slope against ratio between lid and floor rotation rate with a sortation on the average absolute tangential flow velocity.

3.4.4 Transverse slope effect

In Figure 18 the calculated transverse slope effect is shown for 1mm and 4mm grains with floor rotation experiments included. The same pattern as was observed with lid rotation experiments (Figure 14) is observed. Around $\theta/\theta_{cr} \approx 2.5$, where the transition from rolling to saltation was observed, the magnitude of the transverse slope effect indeed increases. Unlike the sudden transition in Figure 14, which apparently is caused by the data gap, this transition is rather gradual.

From the moving mean the coefficients A and B in the function $f(\theta) = A\left(\frac{\theta}{\theta_{cr}}\right)^B$ are derived. These are given in Figure 19. A clear distinction is visible between the rolling, transitional, and saltation phases. The empirical factor A is approximately equal for rolling and saltation. A Large increase in A is observed in the transitional phase, which is caused by the increasing transverse slope effect magnitude. This is also shown by the negative power B during this phase. For both rolling and saltation the power B derived from the moving mean is higher than the power derived from the fit on data of lid rotation experiments (equation (30) and (32)), which implies that the rate at which tan(δ) increases with increasing flow velocity is dependent on the ratio between lid and floor rotation rates. This is likely linked to the difference between calculated flow velocity and actual flow velocity in experiments with floor rotation due to the presence of bed forms as was previously observed from Figure 17.

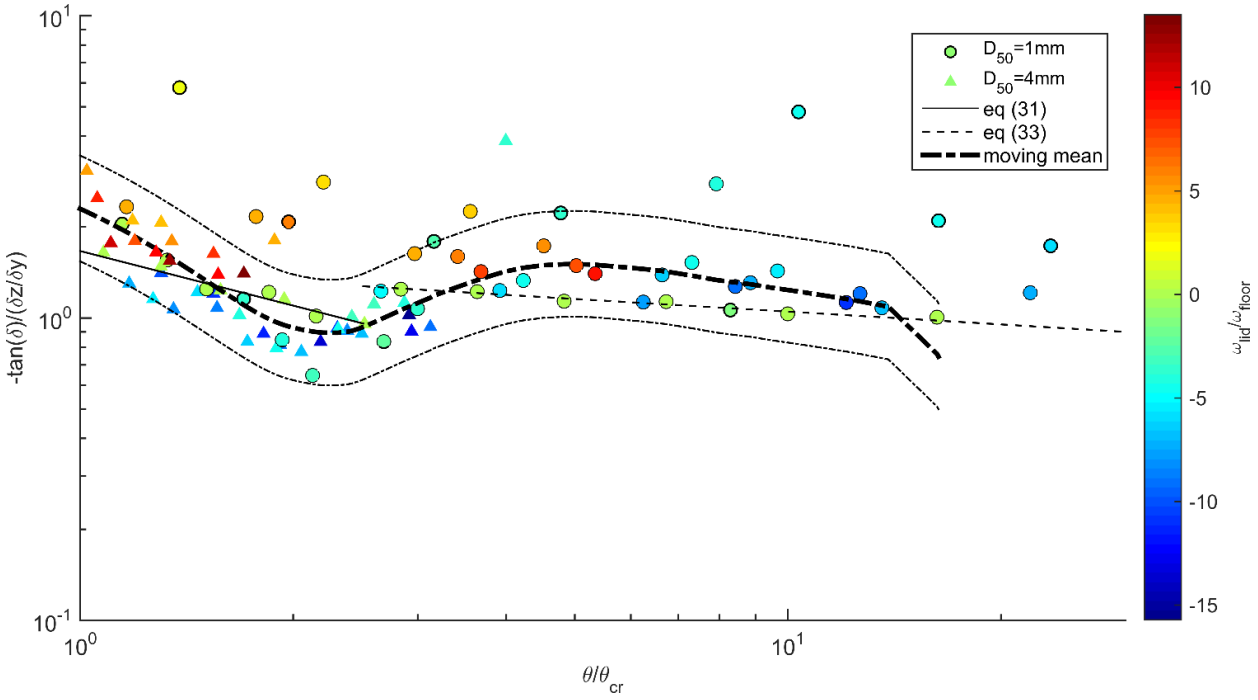

Figure 18, transverse slope effect for 1mm and 4mm grains in a rotating carousel with a moving mean and 50% confidence intervals.

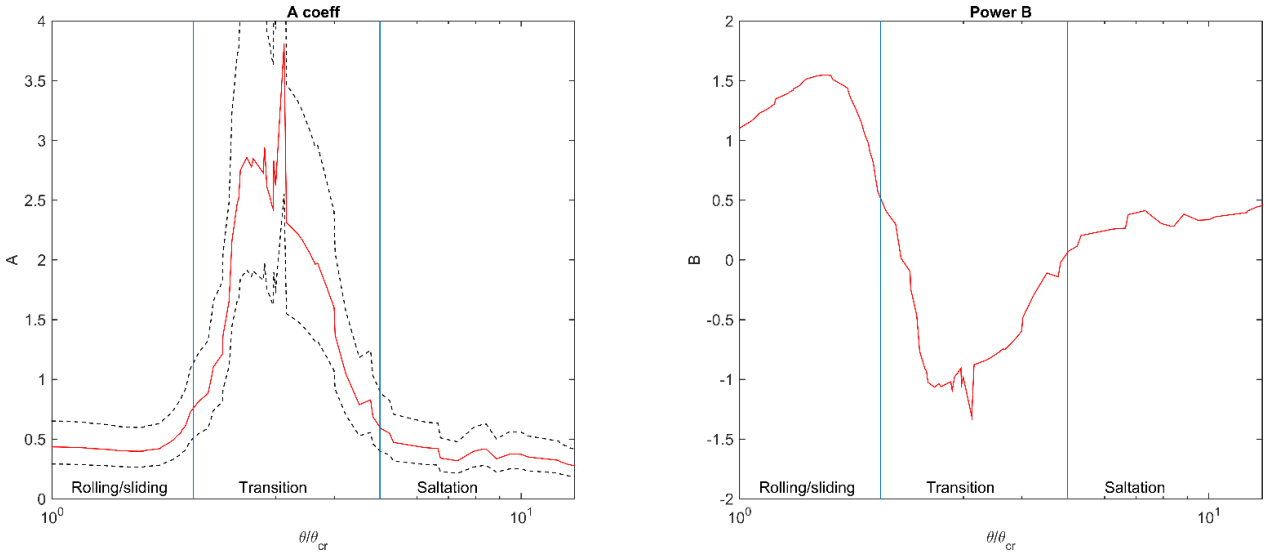

Figure 19, coefficients A and B for the standard function of the transverse slope effect $f(\theta) = A\left(\frac{\theta}{\theta_{cr}}\right)^{B}$ *derived from the moving mean of Figure 18.*

4 DISCUSSION

4.1 INTERPRETATION OF RESULTS AND COMPARISON WITH LITERATURE

A comparison between the data of this study and the resulting transverse slope predictors (equation (30) to (33)) for the different transport modes is given in Figure 20. Towards higher Shields numbers, from θ/θ_{cr}=2.5, a transition is observed from bed load transport to saltation. This transition coincides with a change in the power of $f(\theta)$ to 0.14 and a drop in the steepness of the transverse slope, which is against the trend of an increasing slope with higher Shields numbers. The effect of the transition from rolling to saltation has not been accounted for in existing transverse slope effect models. Sekine and Parker, 1992, used a detailed saltation model (Sekine and Kikkawa, 1992) to derive a model for the transverse slope effect for saltating grains. They found a dependency of Shields' number to $\theta/\theta_{cr}^{0.25}$, which is in agreement with the observed decrease of the power compared with rolling sediment. They however did not account for bed forms in their model, nor did they give a physical reason for the deviation of this power from other transverse slope predictors. In Figure 21, nondimensional saltation height (Bridge and Bennett, 1992) is added to the results for lid rotation. The drop in steepness of the transverse slope coincides with a saltation height of approximately $1.2D_{50}$. As $\tan(\delta)$ remains approximately similar, this drop in steepness implies that the change in transport mode from rolling to bouncing increases downslope velocity of sediment particles. This may be related to the fact that bouncing is more energy efficient than rolling (Erismann, 1985).

For rolling the transverse slope effect in a carousel is similar to that of previous experiments and relations. The power of $f(\theta)$ is slightly larger, 0.6 whereas most studies have shown a dependency to the square root of θ (equation (5)). The larger power implies that in carousels the transverse slope effect strength decreases faster with increasing sediment transport compared to other types of flumes. This implies that the presence of stronger helical flows leads to an increased sensitivity of the transverse slope effect to Shields number. This could be related to the presence of secondary flow in straight flumes, which is viewed as negligible in previous research. As mentioned in section 1.2.8, ignoring secondary flows which are in fact present leads to the under prediction of the transverse slope effect.

A dependence of grain size on the transverse slope effect was observed. The transverse slope effect is stronger for coarser grains. This coincides with observations and transverse slope predictors from previous research (e.g. Talmon et al., 1995; Talmon and Wiesemann, 2006). Similarity between grain sizes was achieved by plotting the transverse slope effect against θ/θ_{cr}. This is a more elegant method than the aforementioned researches as the number of variables and constants is decreased. In Figure 21, a steep slope is observed for a 4mm experiment which has higher calculated saltation height than the saltation height where the transition occurs for 1mm grains. This indicates that grain size influences the saltation height at which the transition occurs, the transition occurs at a higher saltation height for coarser grains. More experimental data of smaller grain sizes and grain sizes between 1 and 4mm are needed to be able to quantify this.

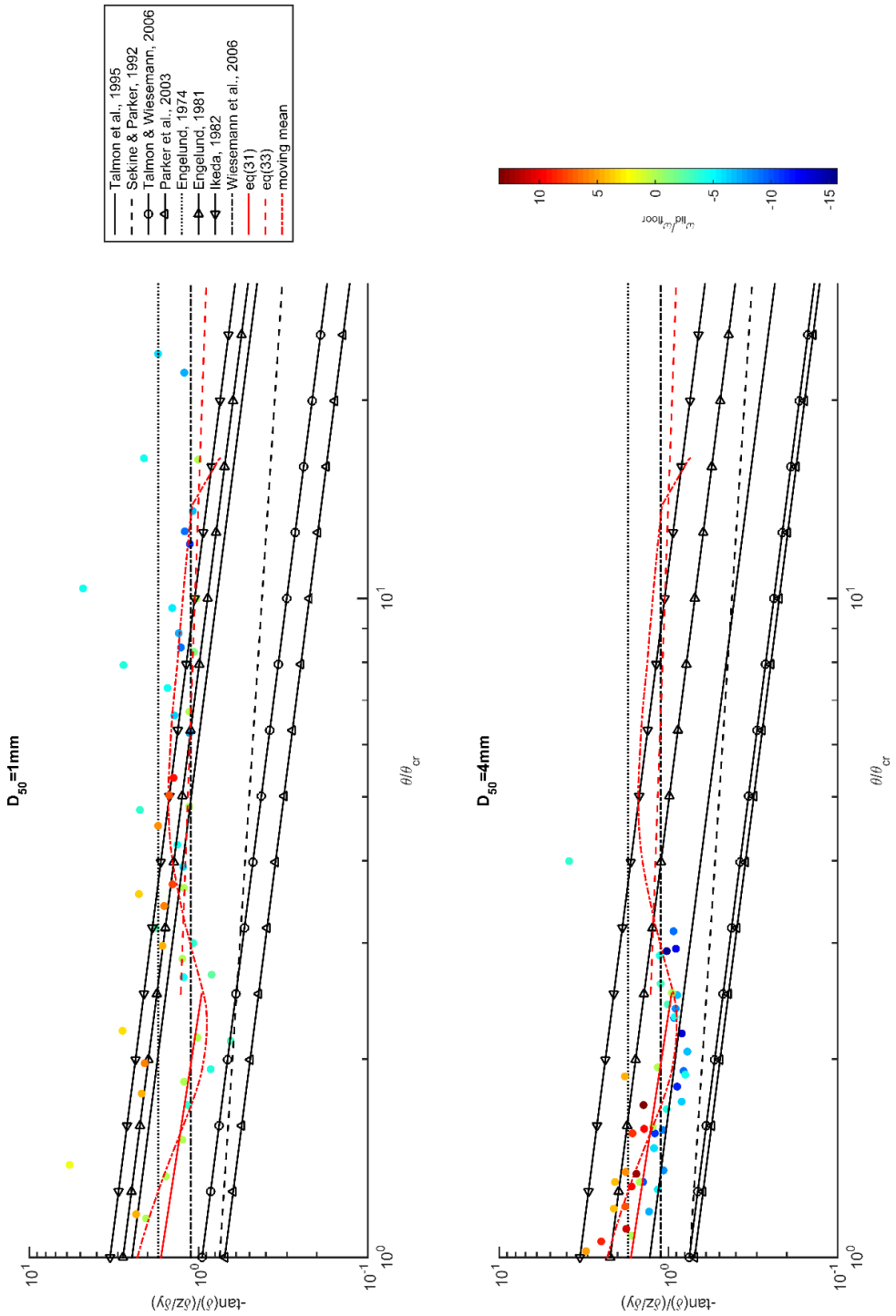

Figure 20, comparison between the data and resulting transverse slope predictors and transverse slope models from literature (Table 1).

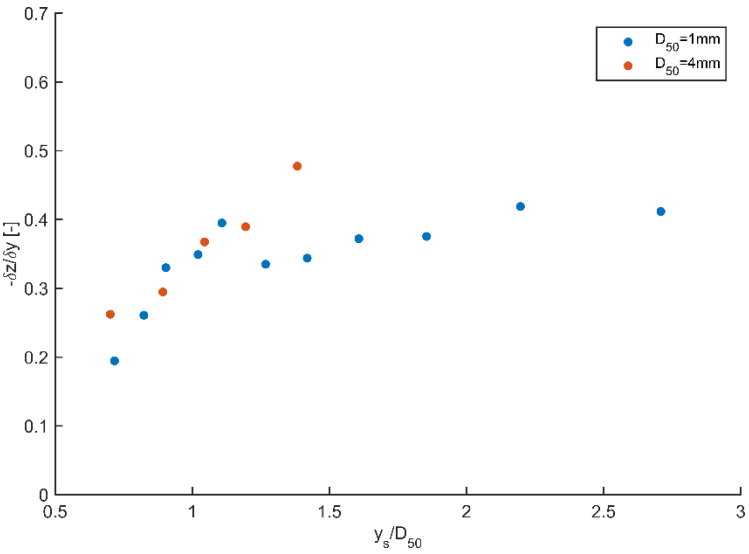

Figure 21, transverse slope against θ/θ_{cr} with nondimensional saltation height (Bridge and Bennett, 1992).

4.2 IMPLICATIONS ON BAR PATTERN MODELLING

The transverse slope effect is one of the most important parameters for the prediction of bar patterns (Schuurman et al., 2013). In models, it strongly influences the predicted braiding index and bar dimensions. In Figure 22, the transverse slope model based on equations (30) and (32) is compared against a transverse slope predictor (Talmon et al., 1995), which is commonly used in bar pattern modelling. The incorporation of the influence of grain size in the transverse slope model leads to the unification of different grain sizes along the chosen x-axis. For rolling bed load transport, the new transverse slope model does not differ much from the model of Talmon et al. (1995), though it will predict a higher braiding index and shorter relative bar length for D_{50}<40mm, and vice versa for D_{50}>40mm. In other words, using the new transverse slope model for sand bed rivers at low Shields numbers will results in model outputs with slightly smaller and steeper bars with deeper channels, as the transverse slope effect is found to be weaker compared to Talmon et al. (1995). After the transition to saltation, which is in fact smooth, the sensitivity of the predicted braiding index and bar length to Shields' number is decreased. Towards higher Shields numbers, the new transverse slope predictor will lead to model outputs with smoother, bigger bars compared to using Talmon et al. (1995) as the bed slope effect becomes stronger.

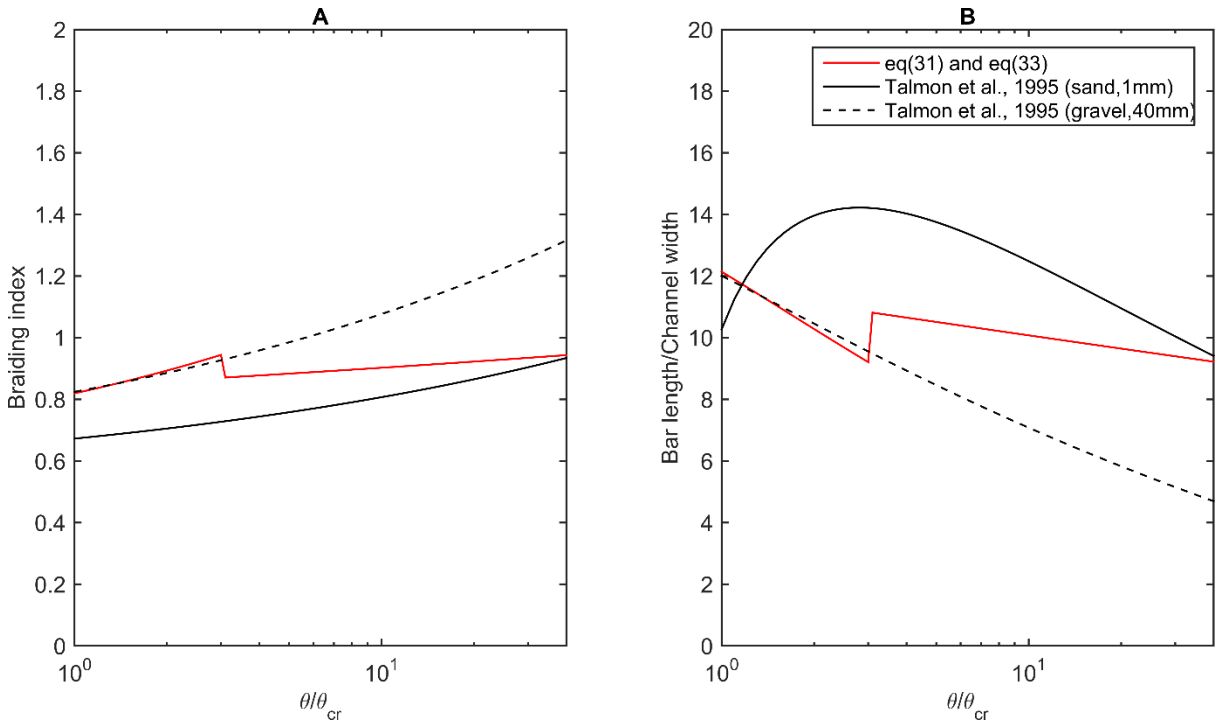

Figure 22, A: Braiding index and B: Bar length divided by channel width against θ/θ_{cr} for a middle of the road river (Kleinhans and van den Berg, 2011; Q=200m/s, W=50m, C=30m$^{1/2}$/s, h=2m) calculated from the theory of Crosato and Mosselman, 2009.

4.3 APPLICABILITY OF A CAROUSEL FOR TRANSVERSE SLOPE EXPERIMENTS

The current approach to obtain experimental data of the transverse slope effect is to perform bed levelling experiments in straight flumes (e.g. Talmon and Wiesemann, 2006, Wiesemann et al., 2006). It is assumed that only straight flume experiments show reliable data as secondary flow may be ignored, which reduces complexity. But the influence of boundary and initial conditions on the results of these experiments is considerable and ignoring helical flow which is in fact present leads to an under prediction of the transverse slope effect (section 1.2.8). For these reasons and reasons given in section 1.2.9 a carousel was chosen to conduct experiments for this research.

The results from experiments with lid rotation indicate that the transverse slope effect can be adequately researched in carousels, as is shown by the R^2 values of equations (30) and (32). The applied methods to solve the addition of floor rotation shows promising results. The same trend in the magnitude of the transverse slope effect for rolling and saltation as in lid rotation experiments is observed. But as of yet it is not possible to derive a transverse slope model from these results due to considerable scatter. As is shown by Figure 17, multiple secondary flow cells cannot be adequately modelled in 1D, therefore a number of experiments could not be used for the derivation of the transverse slope effect. Helical flow was estimated in 1D using the model of Engelund, 1974, which is based on the assumption of a logarithmic flow profile over the z-axis and vanishing shear stress at the water surface. This is in fact not true for carousels. The presence of dunes, which are also deformed due to the curvature of the channel leading to different flow

velocities along the width, strongly affects local flow conditions. Much steeper transverse slopes were observed at the dune troughs compared to the crests, which indicates that dunes troughs enhance helical flow wile crests reduce helical flow. Meanwhile, down channel directed flow velocity is increased at the dune crests and reduced at the dune troughs. Due to the nonlinearity of sediment transport to flow velocity, this highly 3D flow profile has influences on the transverse slope effect which cannot be adequately accounted for using a 1D approach. More detailed 3D flow computations are necessary, a large eddy simulation should be conducted which should be calibrated against detailed flow measurements under the dune regime.

5 CONCLUSIONS AND RECOMMENDATIONS

A transverse slope model was derived from experimental data collected in a carousel with independently rotating lid and floor. This is a more elegant method than bed levelling experiments, on which most of the existing predictors are based. Results are not influenced by chosen initial conditions, and the presence of secondary flow allows for the self-formation of a transverse slope and bed forms.

When sediment is rolling, the transverse slope effect was found to be inversely proportional to Shields' number to the power of 0.6 and the transverse slope's steepness. Towards higher Shields numbers a transition was observed from rolling to saltation. This led to an increase of the slope effect's magnitude and a lower sensitivity to Shields' number, the power was reduced to 0.14. A similarity of the transverse slope effect for different grain sizes was found by plotting the transverse slope effect against Shields' number divided by the critical Shields number for the initiation of sediment transport. The new transverse slope predictor is therefore applicable for a range of grain sizes between 1mm and 4mm under bed load transport. It must however be noted that the transition from rolling to saltation occurred at a higher saltation height for 4mm grains than 1mm grains. More experimental data is needed on grain sizes smaller than 1mm and between 1 and 4mm to find out if there is a relation between grain size and the saltation height at which the observed transition occurs.

The way the formation of transverse slopes in carousels are formed was explored. It was found that transverse slopes in carousels are the result of flow only. Outward centrifugal force on mobile and immobile grains was found to be at least a factor 1000 smaller than inward force by helical flow. Helical flow may be reduced to near zero by counter rotation of the floor at a rate at which the absolute flow velocity in the flume is also near zero. The reversal of the transverse slope's direction is the result of the presence of multiple secondary flow cells.

The high R^2 values of equations (30) and (32) indicate that the transverse slope effect can be reasonably well derived from 1D calculation of helical flow. But for experiments with floor rotation the scatter is much larger. Moreover, multiple secondary flow cells could not be modelled using a 1D approach. Though dunes were present in almost all experiments, the influence they have on the transverse slope effect cannot be adequately studied with the methods applied in this research. Flume averaged helical flow and flume averaged transverse slope angle was used for the derivation of the transverse slope effect. But it was observed that these are highly variable. Helical flow is stronger in dune troughs than at dune crests, resulting in steep transverse slopes in troughs than at dune crests. The nonlinearity of sediment transport to flow will therefore inevitably cause a difference between the length averaged transverse slope effect and actual slope effect. For these reasons it is recommended that a large eddy simulation is conducted so that these 3D effect can be accounted for.

ACKNOWLEDGEMENTS

I would like to thank my supervisors Maarten Kleinhans and Anne Baar for giving me the opportunity to do this research and their continuous support. Conducting experiments in the carousel at TU Delft was possible thanks to cooperation with Wim Uijjtewaal. The technical staff at the Water Lab in Delft: Sander, Jaap, Hans, Frank and Rob continuously worked on improving the experimental setup and prevented me from breaking things. Discussions with Jessica Bergsma, Niels Mulder, and Elise Winden were helpful during the data analysis and writing process.

REFERENCES

Ashida, K., Michiue, M., 1972. Study on hydraulic resistance and bedload transport rate in alluvial streams. Trans. Japan Soc. Civil Engineering 206, 59-69.

Bolla Pittagula, M., Repetto, R., Tubino, M., 2003. Channel bifurcation in braided rivers: Equilibrium configurations and stability. Water Resources Research 39, 1046. DOI:10.1029/2001WR001112.

Bolla Pittagula, M., Coco, G., Kleinhans, M.G., 2015. A unified framework for stability of channel bifurcations in gravel and sand fluvial systems. Geophysical Research Letters 42. DOI: 10.1002/2015GL065175.

Bridge, J.S., Dominic, D.F., 1984. Bed load grain velocities and sediment transport rates. Water Resources Research 20 no. 3, 476-490.

Bridge, J.S., Bennett, S.J., 1992. A Model for the Entrainment and Transport of Sediment Grains of Mixed Sizes, Shapes, and Densities. Water Resources Research 29 no. 2, 337-363.

Crosato, A., Mosselman, E., 2009. Simple physics-based predictor for the number of river bars and the transition between meandering and braiding. Water Resources Research 45, W03424. DOI:10.1029/2008WR007242.

Dietrich, W.E., Smith, J.D., 1984. Bed Load Transport in a River Meander. Water Resources Research 20, 1355-1380.

Edmonds, D.A., Slingerland, R.L., 2008. Stability of delta distributary networks and their bifurcations. Water Resources Research 44, W09426. DOI:10.1029/2008WR006992.

Engelund, F., 1974. Flow and Bed Topography in Channel Bends. Journal of the Hydraulics Division 100, 1631-1648.

Engelund, F., 1975. Instability of flow in a curved alluvial channel. Journal of Fluid Mechanics 72, 145-160.

Erismann, T.H., 1985. Flowing, Rolling, Bouncing, Sliding: Synopsis of Basic Mechanisms. Acta Mechanica 64, 101-110.

Hasegawa, K., 1981. Bank erosion discharge based on a non-equilibrium theory. Trans. Japan Soc. Civ. Engrg. 316, 37-52.

Hirano, M., 1973. Riverbed variation with bank erosion. Trans. Japan Soc. Civ. Engrg. 210, 13-20.

Ikeda, S., 1982. Lateral bed load transport on side slopes. Journal of Hydraulic Division 108, 1369-1373.

Ikeda, S., Nishimura, T., 1986. Flow and Bed Profile in Meandering Sand-Silt Rivers. Journal of Hydraulic Engineering 112, 562-579.

Kleinhans, M.G., 2005. Flow discharge and sediment transport models for estimating a minimum timescale of hydrological activity and channel and delta formation on Mars. Journal of Geophysical Research 110, E12003. DOI:10.1029/2005JE002521.

Kleinhans., M.G., Jagers, H.R.A., Mosselman E., Sloff, C.J., 2008. Bifurcation dynamics and avulsion duration in meandering rivers by one-dimensional and three-dimensional models. Water Resources Research 44, W08454. DOI:10.1029/2007WR005912

Kleinhans, M.G., van den Berg, J.H., 2011. River channel and bar patterns explained and predicted by an empirical and a physics-based method. Earth Surface Processes and Landforms 36, 721-738. DOI:10.1002/esp.2090.

Kleinhans, M.G., Ferguson, R.I., Lane, S.N., Hardy, R.J., 2013. Splitting rivers at their seams: bifurcations and avulsion. Earth Surface Processes and Landforms 38, 47-61. DOI: 10.1002/esp.3268.

Meyer-Peter, E., Mueller, R., 1948. Formulas for bed-load transport. IAHSR 2nd meeting, Stockholm, 39-64.

Miori, S., Repetto, R., Tubino, M., 2006. A one-dimensional model of bifurcations in gravel bed channels with erodible banks. Water Resources Research 42, W11413. DOI:10.1029/2006WR004863.

Odgaard, A.J., Bergs, M.A., 1988. Flow Processes in a Curved Alluvial Channel. Water Resources Research 24, 45-56.

Olesen, K.W., 1987. Bed topography in shallow river bends. Delft University of Technology, Faculty of Civil Engineering.

Schuurman, F., Marra, W.A., Kleinhans, M.G., 2013. Physics based modeling of large braided sand-bed rivers: Bar pattern formation, dynamics, and sensitivity. Journal of Geophyicial Research: Earth Surface 118, 2509-2527. DOI:10.1002/2013JF002896

Schuurman, F., Kleinhans, M.G., 2013. Major Bed Slope Effects Affecting All River Morphodynamics Models.

Sekine, M.S., Parker, G., 1992. Bed-Load Transport on Transverse Slope I. Journal of Hydraulic Engineering 118, 513-535.

Sekine, M., Kikkawa, H., 1992. Mechanics of Saltating Grains. II. Journal of Hydraulic Engineering 118. 536-558.

Struiksma, N., Olesen, K.W., Flokstra, C., De Vriend, Dr. H.J., 1985. Bed deformation in curved alluvial channels. Journal of Hydraulic research 23:1, 57-79. DOI:10.1080/00221688509499377

Talmon, A.M., De Graaff, J., 1991. Bed-levelling experiments with suspended load. TU Delft, Department of Hydraulic Engineering.

Talmon, A.M., 1992. Bed topography of river bends with suspended sediment transport (Doctoral dissertation, TU Delft, Delft University of Technology).

Talmon, A.M., Struiksma, N., Van Mierlo, M.C.L.M., 1995. Laboratory measurements of the direction of sediment transport on transverse alluvial bed slopes. Journal of Hydraulic Research 33:4, 495-517. DOI: 10.1080/00221689509498657

Talmon, A.M., Wiesemann, J.U., 2006. Influence of Grain Size on the Direcion of Bed-Load Transport on Transverse Sloping Beds. Proceedings Third International Conference on Scour and Erosion. Amsterdam, The Netherlands.

Van den Berg, J.H., Van Gelder, A., 1993. A new bedform stability diagram, with emphasis on the transition of ripples to plane bed in flows over fine sand and silt. Spec. Publs Int. Ass. Sediment 17, 11-21.

Van Rijn, L.C., 1984. Sediment Transport, Part III: Bed Forms and Alluvial Roughness. Journal of Hydraulic Engineering 110, 1733-1754.

Van Rijn, L.C., 2011. Principles of Fluid Flow and Surface Waves in Rivers, Estuaries, Seas and Oceans. Aqua Publications, the Netherlands. ISBN: 978-90-79755-02-8.

Wang, Z.B., de Vries, M., Fokkink, R.J., Langeral, A., 1995. Stability of river bifurcations in 1D morphodynamic models. Journal of Hydraulic Research 33, 739-750. DOI:10.1080/00221689509498549.

Wiesemann, J., Mewis, P., Zanke, U.C.E., 2006. Downslope transport (transverse sediment transport). Third Chinese-German Joint symposium on Coastal and Ocean engineering.

Yamasaka, M., Ikeda, S., Kizaki, S., 1987. Lateral sediment transport of heterogeneous bed materials. Trans. Japan Soc. Civ. Engrg. 387, 105-114.

APPENDICES

APPENDIX 1, LIST OF VARIABLES

α	Angle between flow and sediment transport direction
A	Calibration factor for *f(θ)*
C	Chézy coefficient ($m^{1/2}/s$)
D_{50}	Median grain size (m)
F_c	Centrifugal force (N)
g	Gravitational acceleration (m/s^2)
h	Water depth (m)
ks	Nikuradse roughness height (m)
m	Mass of a single grain (kg)
q_b	Sediment transport per unit width ($kg/m^2/s$)
r	Bend radius (m)
Re_p	Particle Reynolds number
u	Local flow velocity (m/s)
u_{av}	Depth averaged flow velocity (m/s)
$u_{av,r}$	Depth averaged flow velocity relative to the bed (m/s)
u_0	Flow velocity at water surface (m/s)
u*	Shear velocity (m/s)
u^*_{cr}	Critical shear velocity for the initiation of sediment transport (m/s)
u_{dune}	Dune migration velocity (m/s)
v	Fluid viscosity
x	Longitudinal coordinate (m)
y	Transverse coordinate (m)
y_s	Saltation height (m)
z_b	Local bed elevation (m)
z	Grain travelling distance above the bed (m)
β, B, a, K	Secondary flow factors
δ	Angle of the flow near the bed in respect to the horizontal

Δ	Dune height (m)
λ	Bed porosity
λ_s	Adaptation length of the bed (m)
λ_w	Adaptation length of the flow (m)
ζ	Z coordinate relative to water depth (0 at water table, 1 at bed)
Γ	Ratio of flume perimeter and width
τ	Shear stress (N/m^2)
ρ_s	Particle density (kg/m^3)
ρ_w	Fluid density (kg/m^3)
θ	Shields' number
θ_{cr}	Critical Shields' number for sediment mobility
φ_b	Einstein number
$\frac{\partial z_b}{\partial y}$	Transverse slope
$\frac{\partial z_b}{\partial x}$	Longitudinal slope
ϵ_0	Eddy viscosity (m^2/s)
ω	Angular velocity (rad/s)
ω_{floor}	Floor rotation rate (rad/s)
ω_{lid}	Lid rotation rate (rad/s)

APPENDIX 2, EXPERIMENTAL DATA

Experiment no.	D_{50} (mm)	ω_{lid} (rad/s)	ω_{floor} (rad/s)	$\frac{\partial_z}{\partial_y}$
1	0.001	0.598	0.000	-0.349
2	0.001	0.598	-0.209	-0.079
3	0.001	0.598	-0.157	-0.176
4	0.001	0.598	-0.126	-0.184
5	0.001	0.598	0.126	-0.300
6	0.001	0.546	0.000	-0.330
7	0.001	0.503	0.000	-0.261
8	0.001	0.503	-0.314	0.221
9	0.001	0.503	-0.209	-0.117
10	0.001	0.503	-0.157	-0.250
11	0.001	0.503	-0.126	-0.238
12	0.001	0.465	0.000	-0.195
13	0.001	0.465	-0.126	-0.164
14	0.001	1.795	0.000	-0.412
15	0.001	1.795	-0.419	0.069
16	0.001	1.795	-0.314	-0.142
17	0.001	1.795	-0.251	-0.229
18	0.001	1.396	0.000	-0.419
19	0.001	1.396	-0.314	-0.095
20	0.001	1.396	-0.209	-0.248
21	0.001	1.396	-0.157	-0.251
22	0.001	1.396	-0.126	-0.288
23	0.001	1.142	0.000	-0.376
24	0.001	1.142	-0.628	0.361
25	0.001	1.142	-0.314	0.011
26	0.001	1.142	-0.251	-0.044
27	0.001	1.142	-0.209	-0.168
28	0.001	1.142	-0.157	-0.215
29	0.001	1.142	-0.126	-0.239
30	0.001	1.142	0.628	-0.295
31	0.001	1.142	0.314	-0.368
32	0.001	1.142	0.209	-0.381
33	0.001	1.142	0.157	-0.400
34	0.001	1.142	0.126	-0.398
35	0.001	0.967	0.000	-0.372
36	0.001	0.967	-0.314	0.130
37	0.001	0.967	-0.251	-0.066
38	0.001	0.967	-0.209	-0.142

39	0.001	0.967	-0.157	-0.187
40	0.001	0.967	-0.126	-0.255
41	0.001	0.967	0.314	-0.335
42	0.001	0.967	0.209	-0.442
43	0.001	0.967	0.157	-0.389
44	0.001	0.967	0.126	-0.404
45	0.001	0.838	0.000	-0.344
46	0.001	0.739	0.000	-0.335
47	0.001	0.739	-0.628	0.345
48	0.001	0.739	-0.251	-0.011
49	0.001	0.739	-0.209	-0.077
50	0.001	0.739	-0.157	-0.167
51	0.001	0.739	-0.126	-0.208
52	0.001	0.739	0.157	-0.321
53	0.001	0.739	0.126	-0.300
54	0.001	0.661	0.000	-0.395
55	0.004	1.963	0.419	-0.419
56	0.004	1.795	0.000	-0.478
57	0.004	1.795	-0.628	0.259
58	0.004	1.795	-0.519	-0.001
59	0.004	1.795	-0.499	-0.052
60	0.004	1.795	-0.200	-0.360
61	0.004	1.795	-0.143	-0.409
62	0.004	1.795	-0.114	-0.387
63	0.004	1.676	0.419	-0.390
64	0.004	1.396	0.000	-0.368
65	0.004	1.396	-0.628	0.247
66	0.004	1.396	-0.419	-0.164
67	0.004	1.396	-0.419	-0.186
68	0.004	1.396	-0.314	-0.256
69	0.004	1.396	-0.209	-0.377
70	0.004	1.396	-0.157	-0.400
71	0.004	1.396	-0.121	-0.401
72	0.004	1.396	0.286	-0.232
73	0.004	1.396	0.190	-0.342
74	0.004	1.396	0.143	-0.351
75	0.004	1.396	0.114	-0.356
76	0.004	1.571	0.000	-0.390
77	0.004	1.571	-0.628	0.266
78	0.004	1.571	-0.370	-0.205
79	0.004	1.571	-0.233	-0.332

80	0.004	1.571	-0.190	-0.350
81	0.004	1.571	-0.143	-0.383
82	0.004	1.571	-0.114	-0.433
83	0.004	1.571	0.370	-0.373
84	0.004	1.571	0.286	-0.391
85	0.004	1.571	0.190	-0.378
86	0.004	1.571	0.165	-0.412
87	0.004	1.571	0.116	-0.397
88	0.004	1.142	0.000	-0.262
89	0.004	1.142	-0.628	0.184
90	0.004	1.142	-0.286	-0.207
91	0.004	1.142	-0.190	-0.226
92	0.004	1.142	-0.143	-0.294
93	0.004	1.142	-0.114	-0.236
94	0.004	1.257	0.000	-0.295
95	0.004	1.257	-0.628	0.194
96	0.004	1.257	-0.286	-0.290
97	0.004	1.257	-0.196	-0.348
98	0.004	1.257	-0.143	-0.298
99	0.004	1.257	-0.114	-0.286
100	0.004	1.257	0.190	-0.245
101	0.004	1.257	0.143	-0.231
102	0.004	1.257	0.114	-0.313
103	0.004	1.047	-0.190	-0.226
104	0.004	1.047	-0.143	-0.228